AD NUMBER

AD894401

NEW LIMITATION CHANGE

TO

Approved for public release, distribution unlimited

FROM

Distribution authorized to U.S. Gov't. agencies only; Test and Evaluation; 15 MAR 1972. Other requests shall be referred to Air Force Space and Missile Systems Organization, Attn: SYAX, Los Angeles AFB, CA 90045.

AUTHORITY

samso ltr, 21 aug 1973

MSO TR 72-78

LARGE-APERTURE WIDE-ANGLE INFRARED SCANNING SYSTEM

by

W. L. Wolfe
J. E. Harvey
B. C. Platt

March 1972

Prepared for the
Space and Missile Systems Organization
Air Force Systems Command
Los Angeles Air Force Station, California

Optical Sciences Center
University of Arizona
Tucson, Arizona 85721

AVAILABILITY NOTICE

Distribution limited to U. S. Government Agencies only; test and evaluation, 15 January 1972. Other requests for this document must be referred to HQ SAMSO/SYAX, AFUPO, Los Angeles, California 90045.

DISPOSITION INSTRUCTIONS

Do not return this copy. Retain or destroy.

REPRODUCTION NOTICE

This report may be reproduced for any purpose of the U. S. Government.

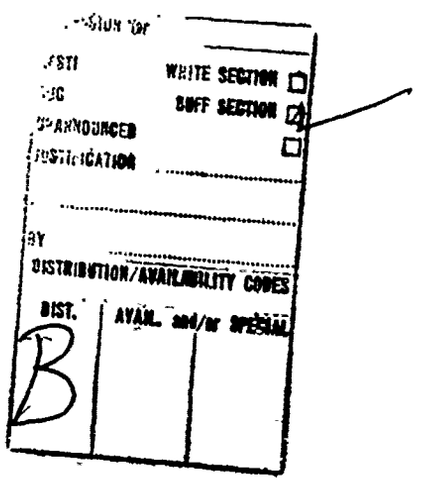

SAMSO TR 72-78

LARGE-APERTURE WIDE-ANGLE INFRARED SCANNING SYSTEM

by

W. L. Wolfe
J. E. Harvey
B. C. Platt

March 1972

Optical Sciences Center
University of Arizona
Tucson, Arizona 85721

FOREWORD

This Final Contract Report of the Optical Sciences Center, University of Arizona, Tucson, Arizona, under U. S. Air Force Contract FO-4701-71-C-0311,was issued by the Department of the Air Force, Space and Missile Systems Organization (AFSC), Air Force Unit Post Office, Los Angeles, California 90045. It is administered by ONRRR, University of Arizona, Tucson, Arizona 85721.

The use of trade names in this report does not constitute an official endorsement or approval of the use of such commercial hardware or software. This report may not be cited for purposes of advertisement.

Publication of this report does not constitute Air Force approval of the report's findings or conclusions. It is published only for the exchange and stimulation of ideas.

Director
Optical Sciences Center

Colonel, USAF
SAMSO (SY)

ABSTRACT

This final report covers a study performed at the University of Arizona concerning large-aperture, wide-angle infrared scanning systems. Both image-plane and object-plane scanning systems were investigated. Two configurations were developed in considerable detail and were shown to present feasible solutions to the specified problem. Laboratory models of these two scanning systems have been constructed to demonstrate the principles involved.

CONTENTS

I. INTRODUCTION

This study is intended to determine the feasibility of building an infrared scanning system with the following specifications:

- Resolution of 3 arc sec.
- Full field of 22°.
- Scanning time of 1 sec.
- Nominal operating wavelength of 3 μm.
- The system should be light, rugged, reliable, and introduce no uncompensated torques or momenta.
- The scan should be essentially linear and unidirectional, with a scan efficiency as large as possible.

From the first two specifications we see that there are 26,400 resolution elements along the width of the full field. Thus, we have approximately 7×10^8 total resolution elements in a square field.

The third specification states that the entire field must be scanned in 1 sec. With 7×10^8 resolution elements and typical detector response times of 1 to 100 μsec it is obvious that many detectors must be used.

The simplest way to scan the field is to use a linear array of detectors and an oscillatory line scan pattern described by

$$X = A \cos(\omega t + \phi).$$

The entire field could be covered in 1 sec if

$$A = 11°, \quad \omega = 2\pi \text{ rad/sec}.$$

The response time of the detectors cannot exceed the minimum time required to scan across the width of one resolution element. Since

$$V = dx/dt = -A\omega \sin(\omega t + \phi)$$

we see that

$$V_{max} = A\omega = 69.2°/\text{sec}.$$

Therefore the required response time is

$$\tau \leqslant 3 \text{ arc sec}/V_{max} = 3 \text{ arc sec}/69.2°/\text{sec} \cdot 1°/3600 \text{ arc sec} = 1.21 \times 10^{-5} \text{ sec}$$

or

$$\tau \leqslant 12 \,\mu\text{sec}.$$

This is a realistic value for the detector response time; however, with a line scan pattern, the detector array must completely span the field in the direction perpendicular to the scanning motion. Hence, allowing one detector per resolution element, a linear array of 26,400 individual detectors would be required.

The large number of detectors involved makes it desirable to use the smallest size available. It is not unreasonable to hope for detectors that are 50 μm in size.

If we allow a 50-μm detector to subtend an angle of 3 arc sec and require that the diffraction-limited blur circle just fill the detector, then the focal length f and diameter D of the optical system are determined:

$$f = 50\ \mu\text{m}/3 \text{ arc sec} = 3.45 \text{ m}$$

$$D = 2.44\ \lambda/3 \text{ arc sec} = 0.505 \text{ m}.$$

Hence an aperture diameter of 0.5 m would be sufficient provided that the radiometric requirements are satisfied and diffraction-limited performance is achieved. However, as a practical consideration, throughout the remainder of this preliminary study we will assume that an effective aperture diameter of 1 m is required.

With a 1-m aperture, we have an $f/3.5$ optical system with a 22° field. This is a wide-angle system and has an image field 1.32 m in diameter.

The following configurations for wide-angle optical systems have been investigated and are discussed in Appendix I.

- One-aspheric Schmidt
- Modified Schmidt
- One-aspheric Wright
- Three-aspheric prime focus
- Three-aspheric Cassegrain–flat field
- Three-aspheric concentric Cassegrain
- Reflective Schmidt
- Refractive Schmidt
- Three-aspheric inverted Cassegrain
- Three-nonrotationally-symmetric aspheric

Refractive systems, despite the advantage of being straight-through, unfolded systems, have the severe disadvantage that suitable materials at the desired wavelength are not readily available in the sizes required.

Conventional reflective systems have obscuration problems because the image field spreads clear across the incident beam in prime focus configurations. The secondary mirror completely obstructs the aperture in Cassegrain-focus configurations.

There are two general categories for scanning systems, object plane and image plane. The particular optical design required will be determined largely by the method of scanning used.

Object-plane scanning systems consist of a scanning mechanism preceding the imaging system, perhaps an oscillating mirror that directs the instantaneous field of view to the desired position in the object field. They have the disadvantage that the scanning mechanism (mirrors or prisms) are usually massive. Hence, at rapid scanning rates, the accelerations experienced by the elements are high and tend to deform optical surfaces. Also the momentum of these moving elements is quite significant and must be compensated.

In image-plane scanning systems the imaging system precedes the scanning mechanism, which then scans the primary image. This can be done by simply moving the detector array across the image plane, or by various more sophisticated techniques of scanning the primary image and relaying the radiation to the detectors. The moving elements in image-plane scanners can often be quite small compared to the system aperture.

Perhaps the greatest difference between object-plane and image-plane scanners is the requirement on the imaging system. In image-plane scanning systems the entire object field must be imaged whereas in object-plane scanning systems, using a linear array of detectors, only a one-dimensional field must be imaged. Hence, there are less stringent requirements upon the imaging system.

II. IMAGE-PLANE SCANNING SYSTEMS

In image-plane scanners the scanning mechanism optically samples the primary image. Hence the primary imaging system must satisfactorily resolve the entire object field.

Conventional image-plane scanning methods include the detector scan, the Nipkow disk, rotating secondary systems, and various other techniques of moving a sampling element in the image plane and relaying the collected radiation to the detectors. Several clever image-plane scanning systems have been reviewed that have small moving parts and simple scanning mechanisms. Most of these systems were designed for use in a moving aircraft, in which the scanning motion is in one direction, and are not easily applied to the present problem.

The detector scan is a promising image-plane scanning technique and has been incorporated into several of the imaging systems mentioned in the introduction. The major disadvantage of the detector scan is the electronic and cryogenic problems that are associated with moving such a large detector array.

Rotating Lens Wheel

A rotating lens wheel provides the possibility of simplifying the system by relaxing some of the requirements on the primary image in hopes of correcting the resulting aberrations with a scanning relay system.

An optical system consisting of a stop at the center of curvature of a spherical primary mirror is the Schmidt configuration without a corrector plate. The chief ray always passes through the center of the stop and therefore through the center of curvature of the primary mirror. Hence the primary mirror is rotationally symmetric with respect to the chief ray for *all* points in the object field. Therefore only spherical aberration results, and it is constant over the entire image field. The image field lies on a spherical surface that is concentric with the primary mirror and whose radius is half that of the primary mirror (see Fig. 1).

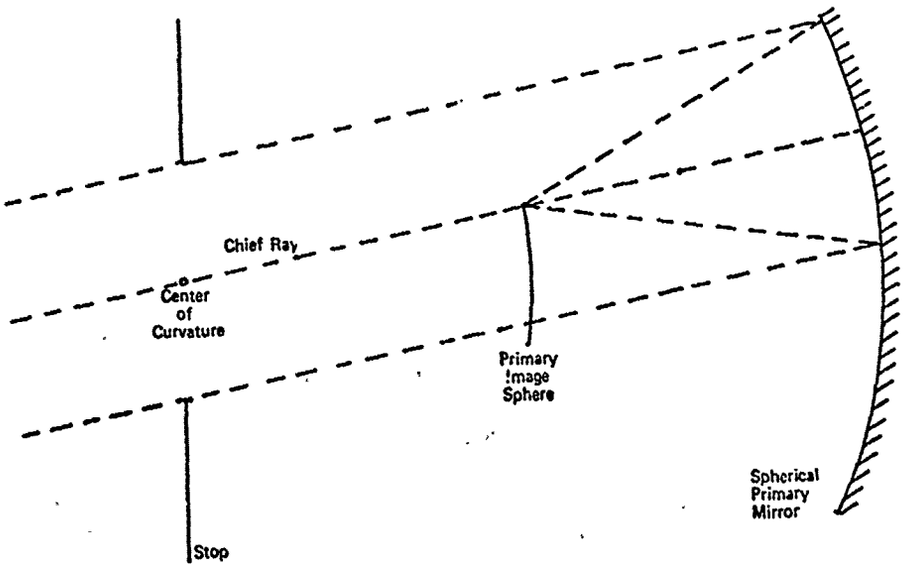

Fig. 1. Schmidt configuration without corrector plate.

In a standard Schmidt system a corrector plate designed to eliminate spherical aberration on axis is placed in the aperture stop. The effectiveness of this corrector plate decreases with field angle owing to the obliqueness of the rays passing through it. Without the corrector plate the primary image has an intolerable amount of spherical aberration; however, the fact that it is constant over the entire image field makes it possible to correct it with a scanning relay system (Fig. 2). The relay system is pivoted about the center of curvature of the primary mirror and relays the instantaneous field of view to the center of curvature.

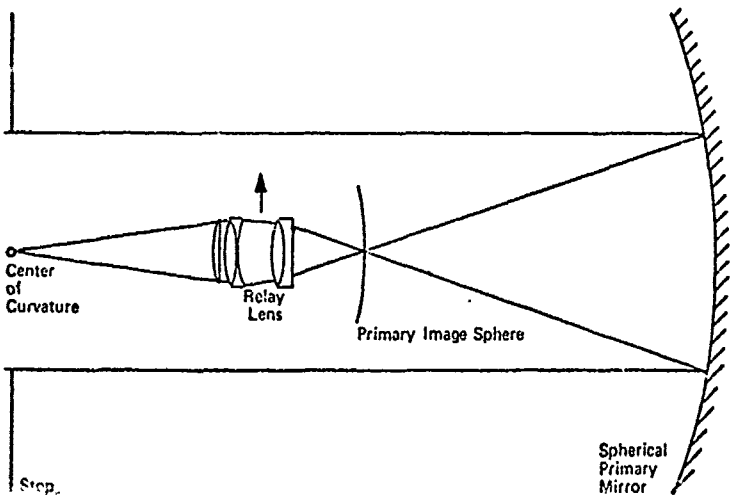

Fig. 2. Schmidt configuration with scanning relay system that corrects the spherical aberration of the primary image.

With an $f/1.5$ primary system, the obscuration due to the primary image is approximately 30%, and there will be no vignetting if the primary diameter is twice that of the aperture stop ($f/0.75$ primary mirror). The relay system can then be chosen to produce an effective $f/3.5$ cone incident on the final image plane.

A refractive relay system similar to a double Gauss or Petzval lens would probably be satisfactory for fields up to 2° or 3°. Furthermore, it may be possible to correct the spherical aberration of the primary image without the use of aspheric surfaces.

For fields of view less than 1.5° reflective relay systems are feasible. Two-mirror and four-mirror reflective relay systems have been investigated using preliminary computer design procedures. The resulting surfaces are not pure conics; however, the higher-order polynomials required are within the realm of current fabrication capabilities.

The two-mirror relay system (Fig. 3) does not have enough degrees of freedom to correct the spherical aberration over the full field without a field lens near the primary image. This system therefore cannot be made totally reflective.

By going to a four-mirror relay (Fig. 4) enough degrees of freedom are available to correct the spherical aberration of the primary image without the need for any refractive elements.

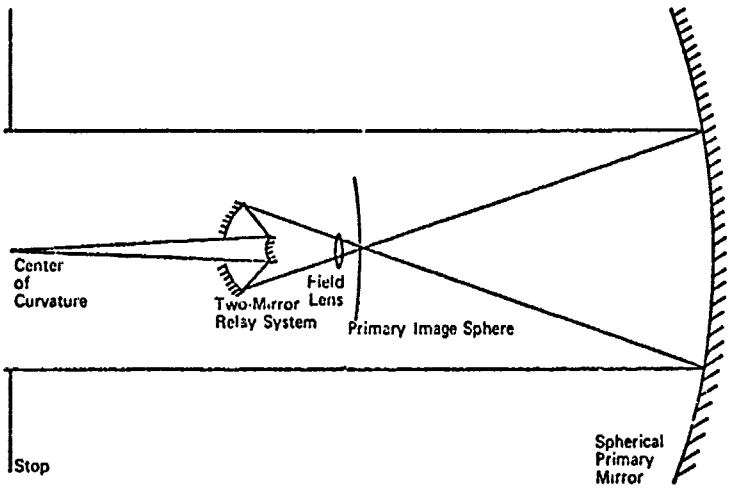

Fig. 3. Two-mirror relay system.

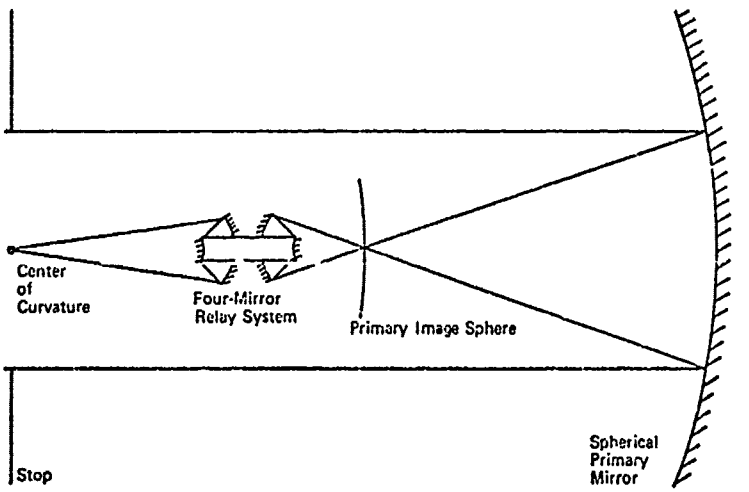

Fig. 4. Four-mirror relay system.

Since a 22° field is to be scanned, 16 relay systems can be placed on the perimeter of a wheel spinning about the center of curvature of the primary image field. By angularly displacing the relay systems on the spinning wheel, a highly efficient faster scan can be produced with 16 lines per frame. A one-dimensional instantaneous field of view of 1.37° can thus be projected onto a linear array of approximately 1500 detectors. A folding mirror placed diagonally in the vicinity of the primary image plane allows the aperture to be in the side of the system enclosure and removes the scanning relay system from the incident beam.

The possibility of further increasing the scan efficiency and reducing the instantaneous field of view by utilizing two primary systems with a single scanning wheel is illustrated in Fig. 5. With this configuration each primary system need only have an 11° X 22° field of view. A single adjustment on the orientation of the folding mirrors will suffice to align the two systems such that they are viewing adjacent portions of the full field. A raster scan with 32 lines per frame is now produced that reduces the necessary field of the relay system to 0.7°. This is not accompanied by an increase in the scan velocity, as two lines are being scanned simultaneously. There is obviously a compromise involved owing to the weight of the additional primary system.

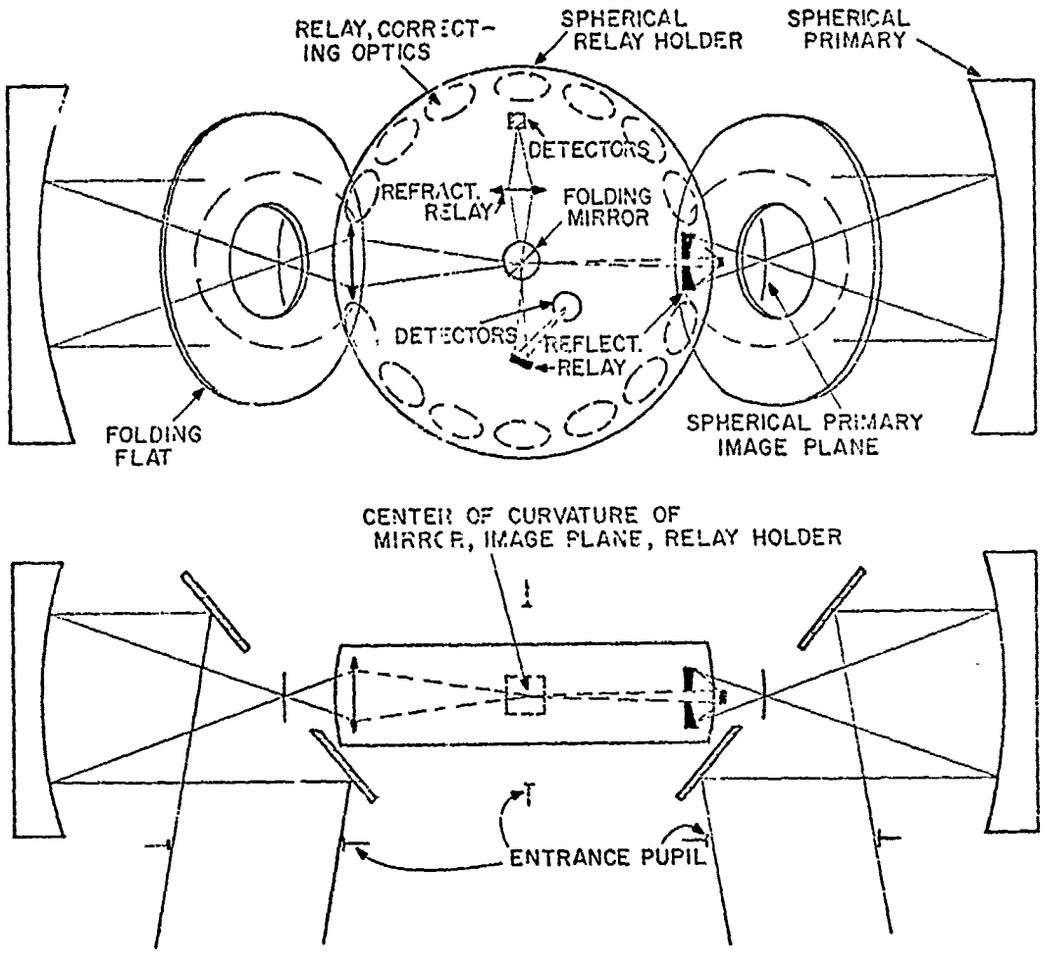

Fig. 5. Rotating lens wheel scanner with two primary systems.

An artist's conception of the complete system with one primary is shown in Fig. 6a. Figure 6b is the same system with two primaries. The system has the following features:

- The scan has constant velocity.
- The scan efficiency approaches 100%.
- The angular momentum is easily compensated with a flywheel.
- Alignment is tedious but straightforward.
- Optical efficiency is high, 100% with $f/0.75$ mirrors.
- There are no oscillations.
- It might be possible to replicate the relay lenses.

A working model of the system with one primary has been constructed (Fig. 7).

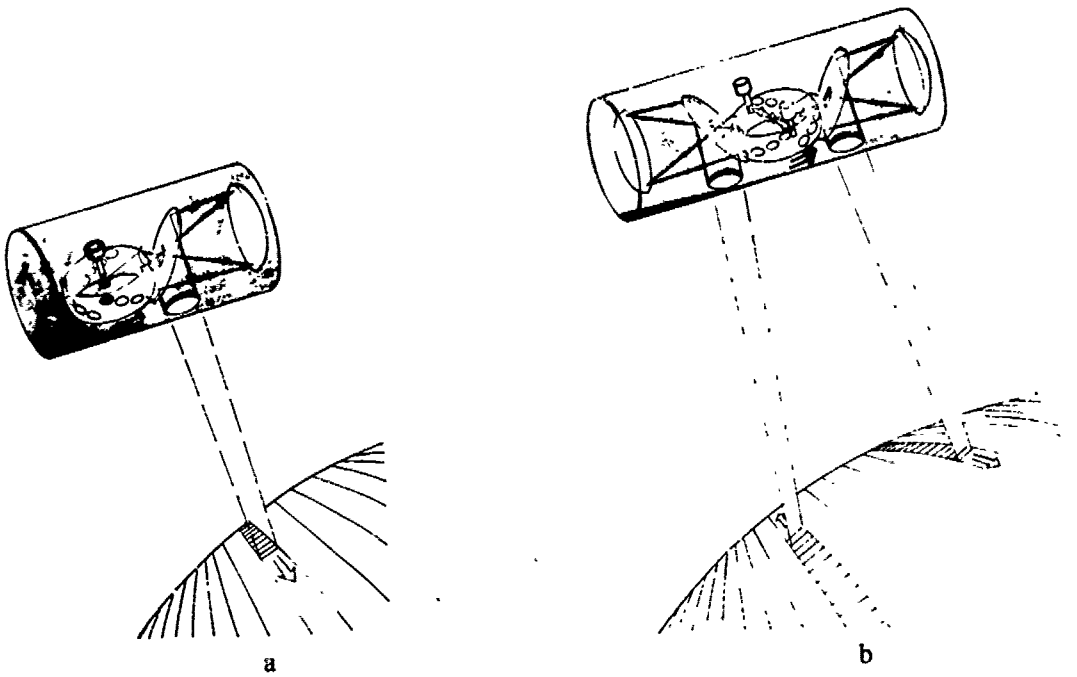

Fig. 6. Rotating lens wheel scanner.
a. With one primary mirror.
b. With two primary mirrors.

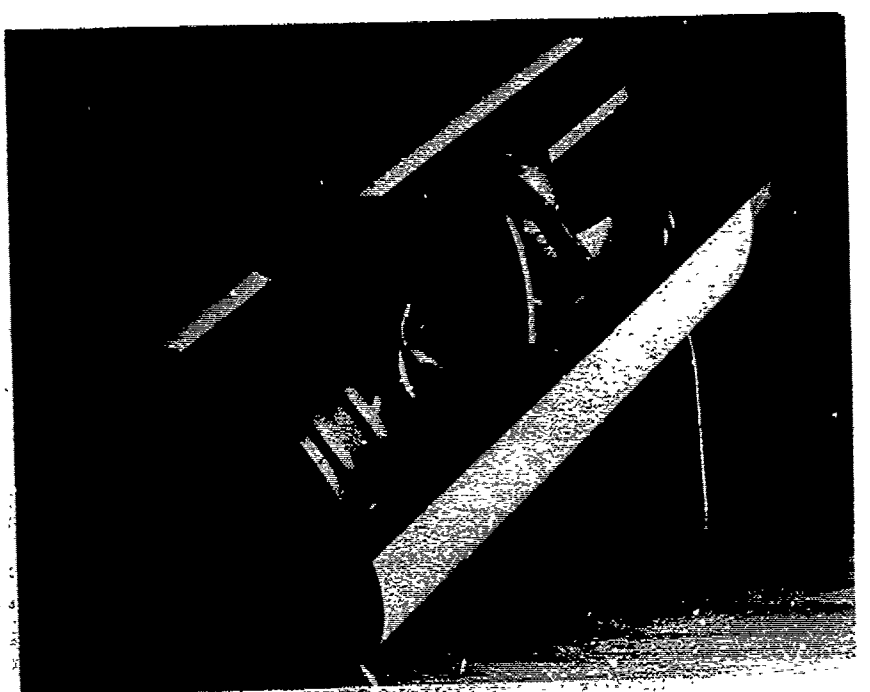

Fig. 7. Working model of the rotating lens wheel scanning system.

III. OBJECT-PLANE SCANNING SYSTEMS

Object-plane scanning systems consist of a scanning mechanism preceding the imaging system that directs the instantaneous field of view to the desired position in the object field.

Oscillating Mirror

Perhaps the simplest object-plane scanning system would consist merely of a single oscillating mirror in front of the imaging system. However, such a system is not momentum compensated, suffers from accelerations that tend to deform the mirror surface, and requires a nonuniform driving force.

Risley Prism Scanner

A Risley prism scanner (see Fig. 8) has the advantage of being a straight-through, unfolded system with no uncompensated momenta, and requires only a simple driving mechanism. However, it has the severe disadvantage that suitable materials for the desired wavelength are not readily available in the sizes required. Fused silica has a problem with water absorption near the operating wavelength. Germanium and silicon are two possible materials, but they are very difficult to obtain in sizes of 1 m or larger in diameter. Also, these refractive materials are subject to radiation damage from the Van Allen belt. Furthermore, the prisms have a mass of approximately 275 kg each for a diameter of 1 m. This weight does not vary much from one material to another, as the less dense materials have a correspondingly smaller index of refraction that requires a larger apex angle (and hence larger volume) to maintain the same deviation.

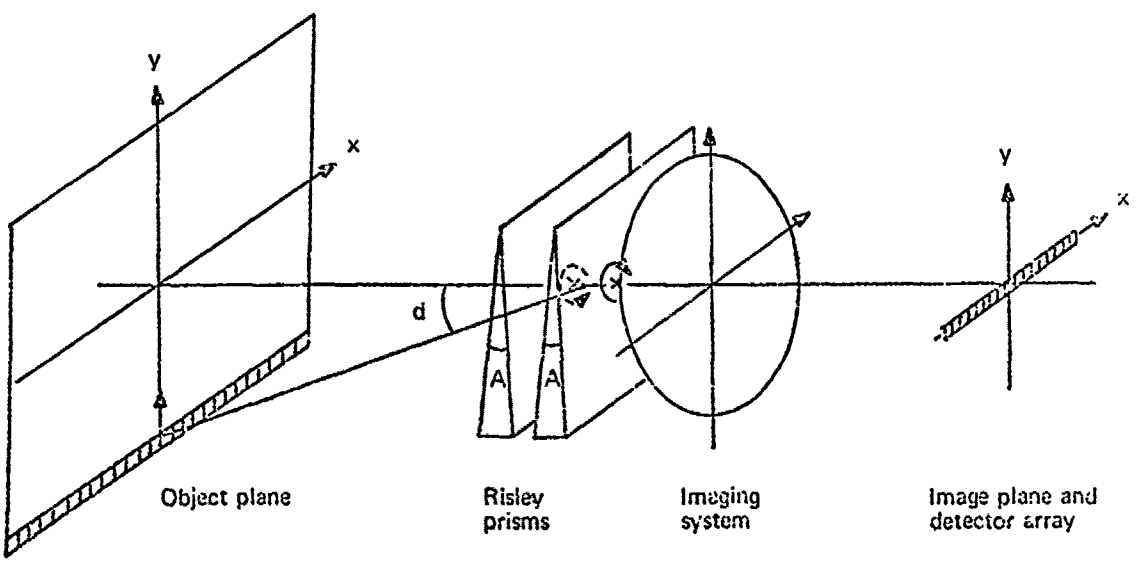

Fig. 8. Risley prism scanner.

Fresnel Risley Prism Scanner

The weight of a Risley prism scanner could be reduced considerably by segmenting the prisms as shown in Fig. 9. This will in general reduce the resolution (i.e., increase the diffraction blur); however, if very stringent requirements on the fabrication of the prism can be met such that $(N-1)Aa = m\lambda$, where m is an integer, then the diffraction properties of the prism in coherent light are unaltered. Since the angular diameter of the instantaneous field of view is approximately equal to the angular diameter of the diffraction blur, the scanner is essentially looking at a point source, and the coherent treatment seems justified. The condition $(N-1)Aa = m\lambda$ can obviously be met for only a single wavelength; hence this is not a reasonable solution if we are working with an appreciable bandwidth or even two discrete wavelengths with an appreciable separation.

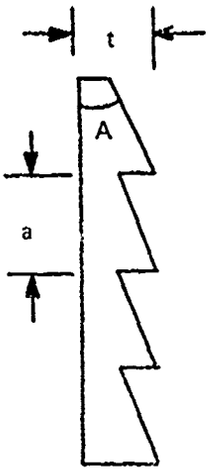

Fig. 9. Segmented prism.

The time-varying effects of the diffraction pattern due to the fact that there are two prisms rotating with respect to each other should be investigated in further detail.

Reflective Risley Scanner

A reflective Risley system can be made by rotating two flat mirrors in opposite directions about parallel axes tilted with respect to the mirror normal (see Fig. 10).

This has the advantage of being an all-reflective system; however, it has the disadvantage that the system must be folded with one of the mirrors off to the side, thus causing enclosure problems. The scanning elements are still large and massive but have simple driving mechanisms and need no momentum compensation.

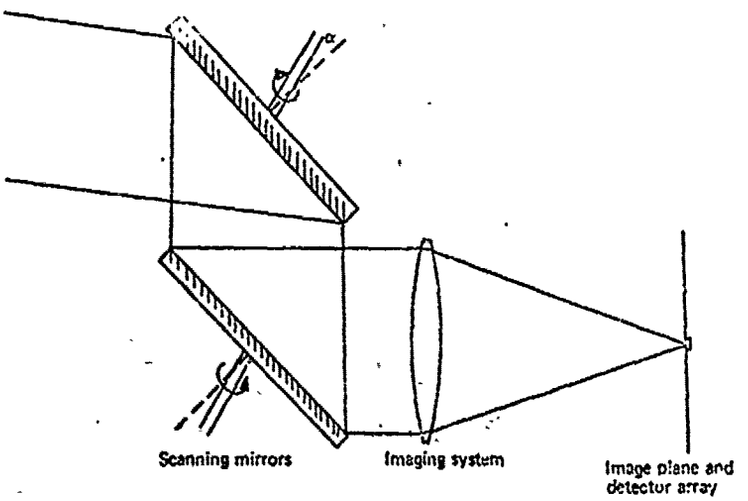

Fig. 10. Reflective Risley scanner.

Reflective Fresnel Risley Scanner

A reflective analog to the Fresnel Risley prism scanner is sketched in Fig. 11. This system has all of the advantages of a Risley prism scanner; i.e., it is a straight-through, unfolded system made up of two identical units rotating in opposite directions. It requires only a simple driving mechanism, has no net momenta or torques, and is only slightly larger than the useful aperture of the system.

The major disadvantage of this system is the monumental engineering feat of fabricating, positioning, and mounting a system of mirrors to within $\lambda/8$. This is necessary, as the system has the same diffraction properties as the Fresnel Risley prism system discussed earlier.

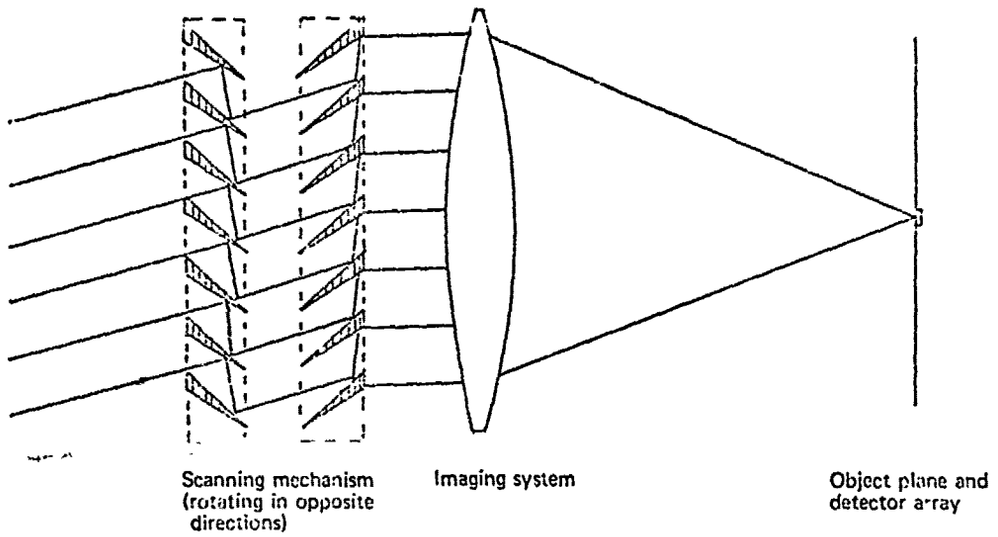

Fig. 11. Reflective Fresnel Risley scanner.

Oscillating/Rotating Mirror (ORM)

The oscillating/rotating mirror can be completely balanced and requires only a constant driving torque. Assume a rotating Z-crank (Fig. 12) carrying two masses, M_1 and M_2, which are swung in a circular path at a radius R_1 from the axis and at a distance D_1 from the center measured along the drive axis. Forces F_1 and F_2 from a couple around point O tending to rotate the system.

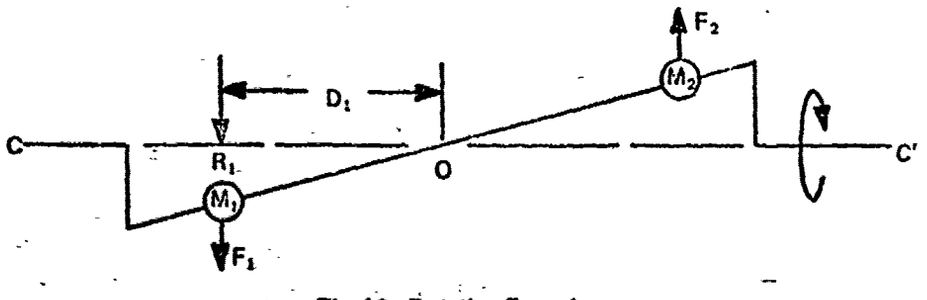

Fig. 12. Rotating Z-crank.

Consider first the masses M_1 and M_2, where $M_1 = M_2$. The inertia of each mass is $I = M_1 R_1^2$. The force F exerted by the rotation of the mass is $F_1 = R_1 M_1 \omega^2$, where ω is the angular speed about CC'. The total couple acting about the center point O due to the rotation of masses M_1 and M_2 is $2F_1 D_1$. The magnitude of the couple is $2M_1 R_1 D_1 \omega^2$.

In Fig. 13 two more masses, M_3 and M_4, where $M_3 = M_4$, have been added to the ends of the crank. By proper choice of these masses and their radii of gyration R_3, a second couple can be produced that will balance the first.

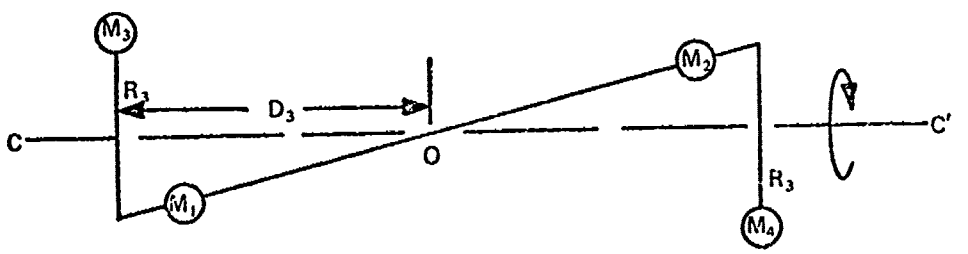

Fig. 13. Rotating Z-crank with two added masses.

Zero torque about O results when $M_3 R_3 D_3$ equals $M_1 R_1 D_1$. This condition is independent of speed since ω cancels out.

If a mirror shaped like a disk is mounted on the Z-crank, it replaces the two masses M_1 and M_2. If the mirror were fixed to the crank it would rotate as the crank rotates and its analysis would be completely analogous to the above case. Assume however, that the mirror is mounted free to rotate about the crank and restrained in an axis orthogonal to the crank axis as illustrated in Figs. 14a and 14b.

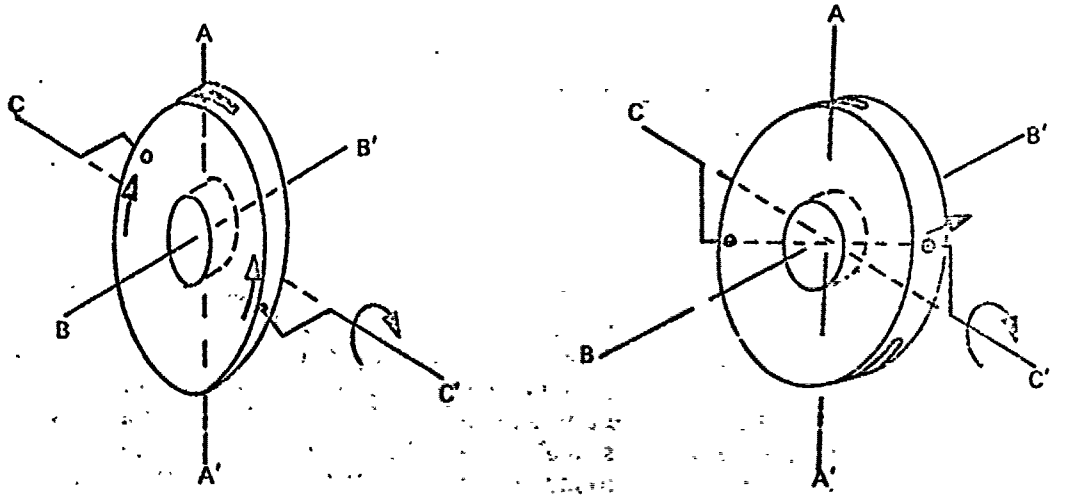

Fig. 14. Oscillating/rotating mirror.
a. Rotating about *B* axis.
b. Rotating about *A* axis.

Figure 14a shows the mirror at one extreme of the excursion of the crank. It is free to rotate about the BB' axis as the crank revolves; it is also free to rotate around the AA' axis as it is pushed to and fro by the crank action. The mirror is constrained to a plane parallel to the AA' axis. In the mode of rotation illustrated in Fig. 14a the inertia of the disk is $I_1 = MR^2/2$ since it is being spun around a central axis. The same disk is illustrated in Fig. 14b after 90° of crank rotation. The inertia of the disk when spun around any diameter is $MR^2/4$. Thus the inertia of the disk changes harmonically as the crank revolves from $I_1 = MR^2/2$ to $I_2 = MR^2/4$. Masses must be added to the system (or removed, in a more sophisticated design) such that total inertia of the mirror will be the same when rotating around both the A and B axes (Fig. 15).

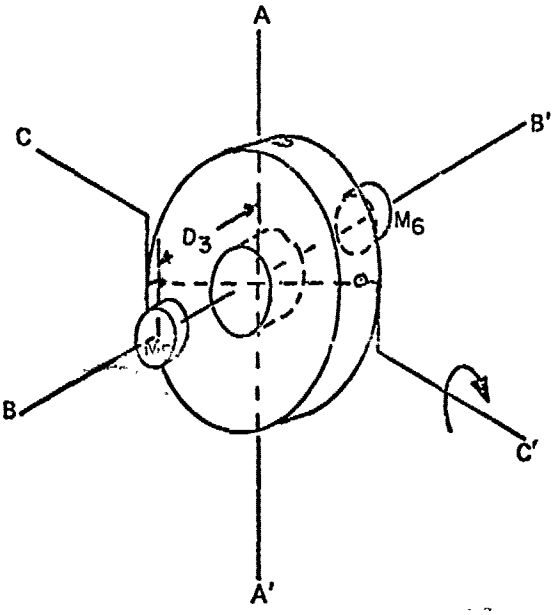

Fig. 15. Oscillating/rotating mirror with constant moment of inertia about A and B axes.

Two symmetrically disposed masses, M_5 and M_6, have been added that move with the mirror and operate at a comparatively large distance D_3 from the AA' axis and at a small distance from the BB' axis. They will thus contribute a larger amount of inertia to the mode illustrated in Fig. 14b than they do to the mode illustrated in Fig. 14a. The inertia added to the system around the A axis by these weights is $I_A = 2M_5D_3^2$. To a first approximation the added inertia around the B axis is small and can be neglected and, because of the AA' restraint, there is no rotation at all around the CC' axis. If the distance D_3 and the masses M_5 and M_6 are properly chosen, the total moment of inertia of the mirror will be constant around both the A and B axes, and the driving torque required around the CC' axis will also be constant.

When the inertia of the mirror has been equalized around both the A and B axes, the system is reduced to the simple diagram shown in Figs. 12 and 13. The counterweights added to Fig. 13 must now produce a couple that is equal and opposite to the couple produced by the mirror and its center balance weights. This means that the inertia of each crank counterweight about the CC' axis must be half the inertia of the mirror, measured with respect to the same axis.

The 45-cm Model

The ORM scanner has been modeled in a 45-cm-diameter aperture to demonstrate that such a structure can be balanced; and driven easily at high speeds (20 Hz). The assembly drawing of the model is shown in Fig. 16. The mirror and the frame are constructed of aluminum, the counterweights of lead, and the bearings and the crank of stainless steel. Both the central weights and the crank counterweights are adjustable to enable final dynamic balance after assembly. The drive motor, not shown in Fig. 14, is attached to the outer frame and drives the Z-crank through a friction clutch and level gear.

A Mirror on One Side of the A Axis

The 45-cm model is a balanced mirror, symmetrical around the A axis. It can easily be shown that the mirror can be nonsymmetrical and still be capable of the same kind of dynamic balance. Figure 17 shows a mirror design that is not symmetrical around the A axis. The mass of the mirror, represented symbolically by two mass points M_2, is first compensated for by the masses M_3 and M_4, which are located on the other side of the AA' axis. The two masses (M_3 and M_4) are chosen to have the same inertia in rotation both around the A axis and the B axis as does the mirror mass. Then the masses M_1 are added along the B axes as before to equilize the inertia of the total mirror (M_2 and M_3) around the A and B axes. Finally, the crank counterweights are added to remove the couple. The system is then balanced as before.

Bearing Friction and Power Requirements

Throughout the mechanical analysis given in this report, it was assumed that all bearings were frictionless and that there was no elastic hysteresis in any of the structural elements that are subjected to time-varying stresses. Under these conditions no driving power would be required. Such is not the case: All bearings have friction; all structural materials exhibit measurable elastic hysteresis. Elastic hysteresis can be ignored as the power required to overcome it will be trivial. However, bearing friction cannot be ignored. It is appropriate to estimate how much power is required to overcome bearing friction and maintain motion in the moving mirror, and to inquire what effects these friction losses may have on the operation of the system. First, consider friction in the bearings. One method of evaluating this loss is to consult with bearing manufacturers, choose appropriate coefficients of rolling friction, compute the loading on each bearing, and calculate the resulting friction loss.

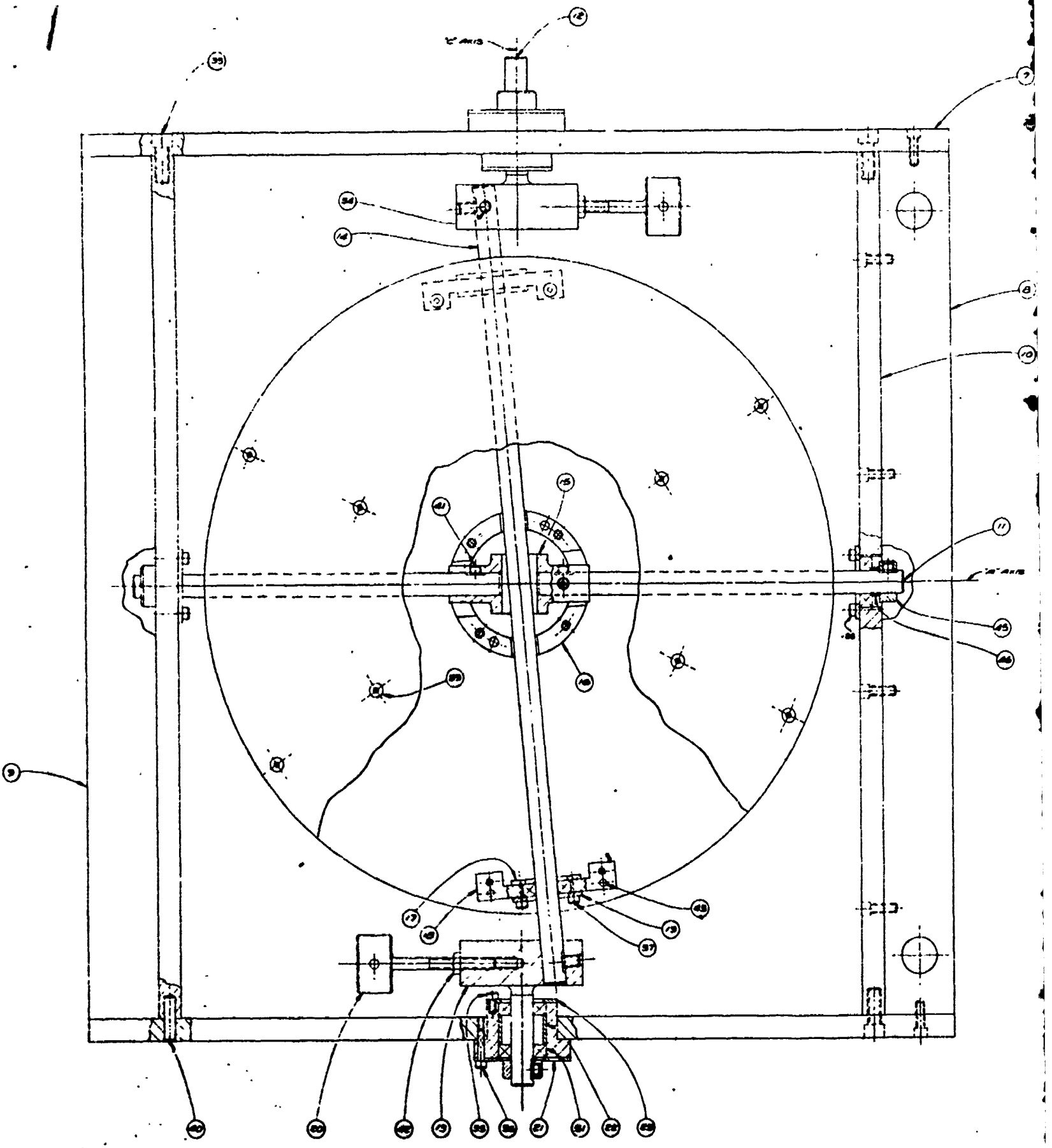

2

Fig. 16

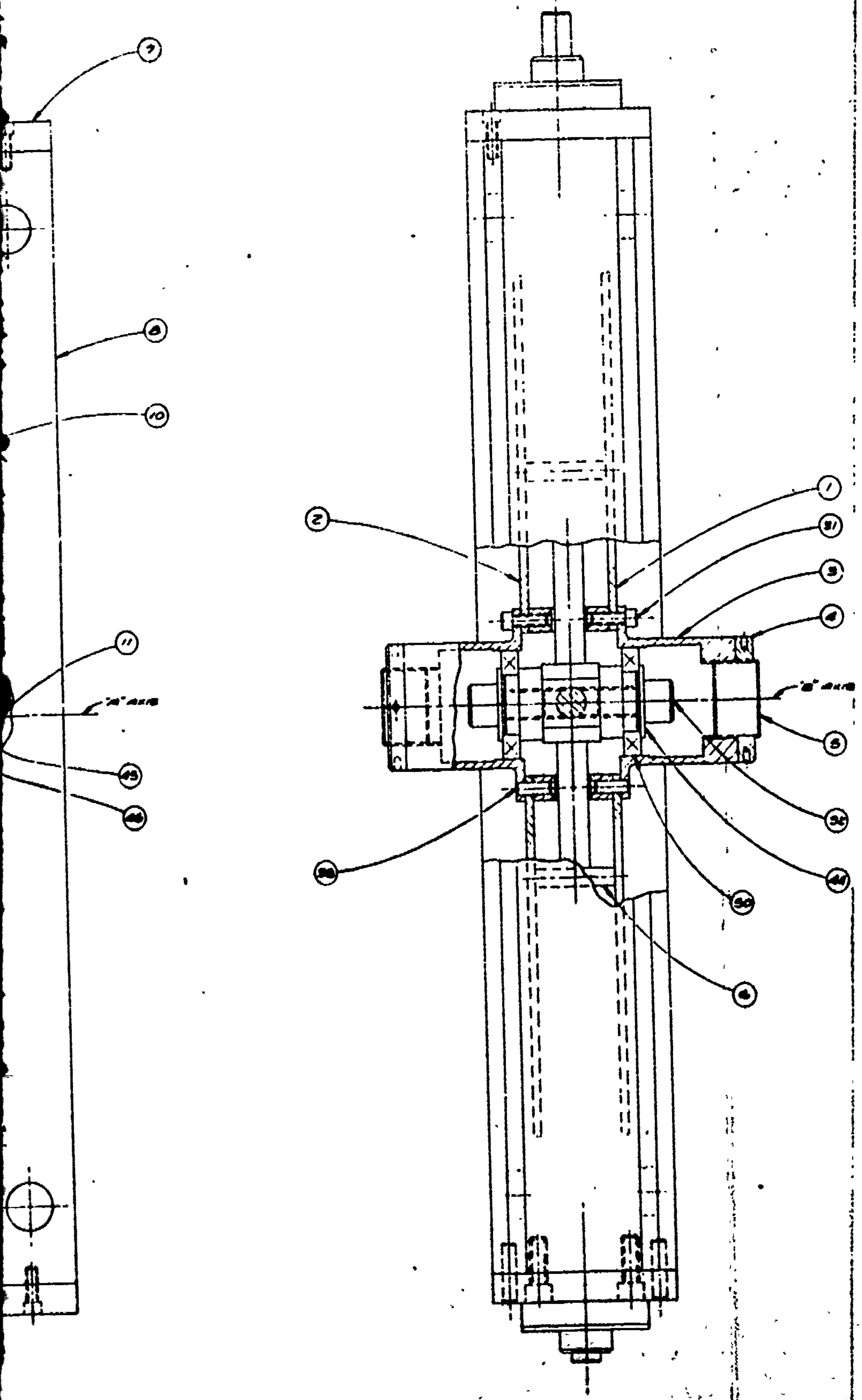

QTY REQ.		DESCRIPTION	CAT. OR DRAWING NUMBER	ITEM
8		BALL BEARING	[illegible] # 87KDD	51
2		BALL BEARING	[illegible] # 31EK	50
				49
				48
				47
8		WASHER	BOSTON # 18036	46
4		COLLAR	BOSTON # 89C62	45
2		WASHER	BOSTON # 18848	44
4		DOWEL	1/8 DIA. × 1/2	43
2		JAM NUT	5/16-18	42
4		SOCKET SET SCREW	5/16-18 × 3/8 LONG	41
6		DOWEL	3/16 DIA × 1 1/4	40
10		BINDING HEAD SCREW	#10-32 × 5/8 LONG	39
4		DOWEL	1/4 DIA. × 3/4	38
8		SOC. HD CAP SCREW	#10-32 × 5/8 LONG	37
8		SOC HD CAP SCREW	#10-32 × 1/2 LONG	36
14		SOC HD CAP SCREW	#10-32 × 3/8 LONG	35
4		SOCKET SET SCREW	5/16-18 × 1/2 LONG	34
8		SOC HD CAP SCREW	3/8-16 × 1 0 LONG	33
2		SOC HD CAP SCREW	5/8-11 × 1 0 LONG	32
32		SOC HD CAP SCREW	1/4-20 × 5/8 LONG	31
				30
				29
				28
				27
				26
				25
				24
[illegible]		BRG RETAINER		23
[illegible]		[illegible] SPACER		22
[illegible]		BRG RETAINER		21
[illegible]		"B" AXIS WEIGHT		20
[illegible]		[illegible]		[illegible]
[illegible]		[illegible]		[illegible]
[illegible]		[illegible]		[illegible]
[illegible]		[illegible]		[illegible]
[illegible]		[illegible]		[illegible]
[illegible]		[illegible]		[illegible]
[illegible]		[illegible]		[illegible]
[illegible]		[illegible]		[illegible]
[illegible]		[illegible]		[illegible]
[illegible]		[illegible]		[illegible]
[illegible]		[illegible]		10
[illegible]		[illegible]		9
[illegible]		[illegible]		8
[illegible]		[illegible]		7
[illegible]		SPACER		6
[illegible]		[illegible]		5
[illegible]		LOCK RING		4
[illegible]		[illegible]		3
1		[illegible]		2
1		[illegible]		1

PACIFIC INFRARED SYSTEMS COMPANY

SCALE MODEL ROTATING/OSCILLATING MIRROR

DWG NO. D 3134-1

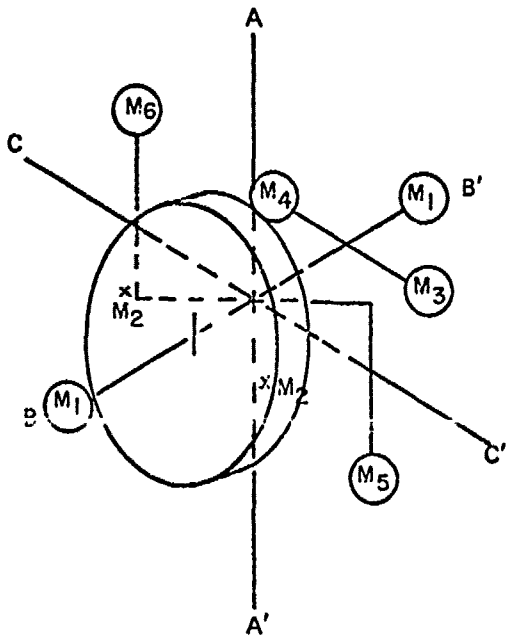

Fig. 17. Oscillating/rotating scanner with mirror on one side of A axis.

In this study, a much less time-consuming method was used. The total kinetic energy E of a body rotating about axis AA' at ω rad/sec and whose rotational moment of inertia about axis AA' is I (m kg sec^2) is given as

$$E = \tfrac{1}{2} I\omega^2 \text{ (watt seconds).}$$

Assume a body of mass 500 kg having a radius of gyration of 1 m. These numbers are offered as being appropriate for a 2.5-m mirror of lightweight design. The moment of inertia is then 500 m kg sec^2. If the body moves in a simple harmonic motion of amplitude 0.1 rad (i.e., total motion of 0.2 rad, or 11.4°) at a frequency of 10 Hz, the maximum angular speed ω is 2π rad/sec. The corresponding kinetic energy is

$$\begin{aligned} E &= \tfrac{1}{2} I\omega^2 \\ &= \tfrac{1}{2} \times 500 \times (2\pi)^2 \\ &= 10{,}000 \text{ W sec.} \end{aligned}$$

Since the kinetic energy is continually passed back and forth between the two modes of vibration, this energy input is required to bring the proposed complete mirror system from rest up to an operational speed of 10 Hz.

It is suggested that, with careful design, the Q (the ratio of the total oscillational energy to the total loss of energy during each complete cycle) of an ORM scanner system of this size should be at least 100. Once the system is set in motion, the power required to operate the mirror would be less than 10,000/100 or 100 W.

The scaling laws for power consumption are of interest. The moments of inertia of geometrically similar bodies scale as the fifth power of the linear dimensions. Thus, at an identical frequency the power required to operate a 1/5-scale (0.5-m aperture) model of the 2.5-m system might be as small as $100\ W \times 0.2^5$, or a few hundredths of a watt.

In practice this value, a small fraction of a watt, is unbelievably small. The earth-based model will require power to overcome air drag and will have bearing friction due to gravity-induced loads, items not existing in orbit. Also neither of these losses follows the fifth power scaling law of the vibration loads.

A Balanced Linear Scan

The 45-cm scale model of the oscillating/rotating mirror was built to be driven in a simple mode, producing a first harmonic or sinusoidal scan. This means that the dwell time changes in a first harmonic manner as the line of sight moves across the field and that the time from point to point similarly changes sinusoidally.

Because of electronic processing techniques involving a multiplicity of delay lines, it is very desirable that the line of sight advance linearly, within limits, across the scan field. This requirement has been defined as linear within ±1% throughout as large a usable range as possible. It will be shown in the analysis that follows that a usable range or scan efficiency of better than 70% can be achieved, the rest being consumed in turnaround time by the introduction of a small amount of third harmonic into the motion, while still maintaining a completely balanced system requiring constant torque.

This scan, being independent of frame time, can be run at 1 Hz or 10 Hz (20 frames) with equal facility. It can be changed from one speed to another with a small expenditure of energy, and because it acts like a flywheel, its motion at any speed takes only a small effort to maintain.

A linear scan can be represented by a straight line up and down from the origin, $y = Ax$. A sinusoidal scan $y = B \sin x$ departs from the straight line as shown in Fig. 18. At any point the departure of the sinusoidal scan from the straight line can be described, $\Delta y = Ax - B \sin x$.

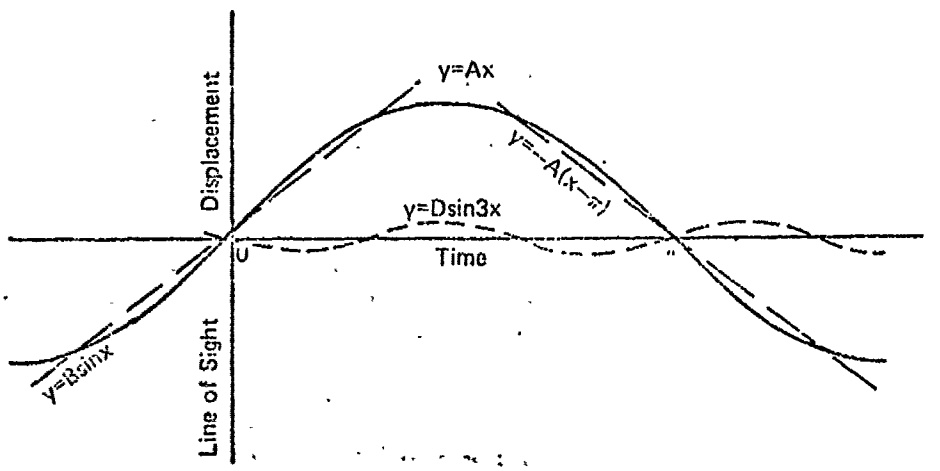

Fig. 18. Representation of fundamental and third-harmonic motion used to approximate a linear scan.

From Fig. 18 it can be seen that the motion that is required to correct the sinusoid in the region around the origin to more closely approach a straight line is the dotted curve D. This required correction is approximately $D \sin 3x$ where the amplitude D is approximately equal to -0.068. At any point the residual, the straight line minus the first plus third harmonic scan, is

$$\Delta y = Ax - \sin x - D \sin 3x.$$

It will be shown that the above residual or scan error, Δy, remains within $\pm 1\%$ or less over about 4.5 out of 2π rad (6.28) (about 72% of the scan) when D is set at -0.068 and A, the straight line slope that is to be approximated, is set at the proper value, 0.826.

To find A, set $\Delta y = 0$ at $x = \pi/3$ (60°) and substitute in the above equation, where $3x = \pi$, $\sin 3x = 0$

$$0 = A(\pi/3) - 0.866$$

$$A = +0.826.$$

Now compute the value of D for maximum permissible error ($\Delta y = -1\%$) at $x = \pi/4$ (45°), which is approximately the point where the curves $\sin x$ and $-\sin 3x$ fit least well:

$$-0.01 = 0.826\pi/4 - 0.707 - 0.707D,$$

$$D = -0.068.$$

As a check, compute the residual at $x = \pi/6$(30°):

$$\Delta y = 0.826\pi/6 - 0.500 + 0.068 = +0.001 \text{ (i.e., 0.1\%)}.$$

Check again at $x = 1.134$ (65°):

$$\Delta y = 0.826 \times 1.134 - 0.906 - 0.0176 = +0.012 \text{ (i.e., +1.2\%)}.$$

Thus, the scan is just going out of tolerance at 65°.

When the scan returns down the next slope of the "triangular" wave, it will again approach a linear function. This time the straight line to be approximated is $y = -A(x-\pi)$. This descending line, the idealized return scan, is also shown in Fig. 18. Substituting this expression into the equation, we again find a small residual

$$\Delta y = -A(x-\pi) - B \sin x - D \sin 3x.$$

The sine functions for the arguments, x and $3x$, are everywhere identical to the values for $x+\pi$ and $3x+\pi$ except for a reversal of sign. Thus, the result is the same small residual although of opposite sign in the interval π through 2π.

For example, check the residual at $x = (7\pi/6)$ (i.e., 210°):

$$\Delta y = -0.826 \times (7\pi/6) + 2.598 + 0.500 - 0.068$$

$$= -0.001 \text{ (i.e., } -0.1\%).$$

It has been shown earlier that the first harmonic motion can be balanced completely with a series of counterweights introduced into the 45-cm model. It is generally true in mechanical systems that harmonic motions can be treated independently. If the first harmonic is balanced and if the third harmonic motion, presumably superimposed upon it by means of a differential, is also balanced, then the resultant of the combination is balanced. This design is no exception. Introduction of a small amount (−0.068) of third harmonic does not disturb the fundamental balance but does require the introduction of a minor third harmonic balance. This can be done in the mechanical input system.

Figure 19 is a schematic drawing of a gear motion that accomplishes the first plus third harmonic drive. This mechanism can be completely balanced. This assembly can be added to the 45-cm model. Gear *A* is stationary, being fixed to the side of the frame. This drive enters through a central axis to arm *B*, which drives a pair of planetary gears, *C*, and another gear, *D*, from which the motion is transferred to the Z-crank axis.

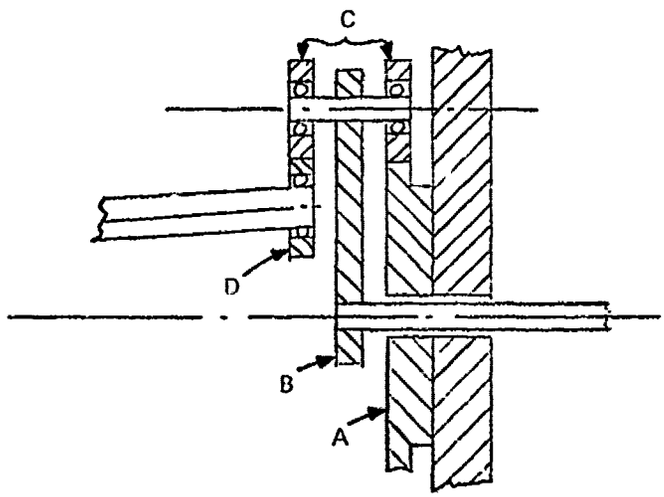

Fig. 19. Planetary gears used to introduce third-harmonic motion.

The gear ratio existing between *A* and *C* is 3:1. Consequently, any point on the face of gear *C*, offset from the gear center, describes a third harmonic whose amplitude is controlled by the amount of offset. In this case the total fundamental excursion of the crank, the amplitude of the fundamental, is taken as 1.0, and the tentative best solution to realizing a scan having less than 1% error 72% of the time is offset, $D = -0.068$.

The third harmonic motion must be balanced independent of the first harmonic balance by the addition of a weight, *E*. When this is done, the total assembly is balanced for both first and third harmonics and should coast like a flywheel, having only losses due to mechanical hysteresis and bearing friction.

This mechanical system is independent of speed. Properly balanced it will run at 30 Hz as well as at 5 Hz, granted that its size is commensurate with reasonable rim accelerations and that elastic hysteresis losses are below the elastic limits of the mirror and bearing materials.

A further requirement is that whatever the mirror and bearing structure stresses may be during the turnaround, the vibration must be damped out before the mirror leaves the dead-time portion of the cycle. Computer techniques will be required to design an optimized mirror structure that withstands these stresses and maintains its figure with the least over-all mass.

The ability to change scanning speed represents a major and fundamental difference between this scanning concept and others that generically consist of drives with "bumpers" on either end of the scan. However well the bumpers may be designed, they are fundamentally springs, and consequently have time constants and characteristic and invariant frequencies. The operation of such systems cannot be made independent of scanning speed, and they can be optimized for two frequencies only with difficulty. This system, a first-plus-third harmonic drive, can operate at any speed at the option of ground control with substantially no change in performance and with very little increase in power input requirements.

Third Harmonic Adjustment and Balance

The third harmonic drive is built with an adjustable amplitude, and further, by means of engaging the gears at one tooth or another, the phase of the third harmonic component can be adjusted. This means that in the experimental model, one is not only able to create a properly adjusted scan that is linear to 1% over 70% of the total scan, but one can also create a scan—with the third harmonic component improperly adjusted—where the departure from linearity can approach 10%.

In proper adjustment the third harmonic component is 180° out of phase with the fundamental component at the center of the field (see Fig. 20) and mathematically at least the amplitude of the third harmonic component is roughly 0.068 times the amplitude of the fundamental. It is thus necessary to make the third harmonic adjustment in both phase and amplitude and to check the results with a systematic measurement of the scan error. However, this adjustment need not be made variable since the design theory is straightforward and since the degree of correction (1%) involved is grosser that the aggregate tolerances in the parts. Consequently, this "adjustment" will be eliminated in future models.

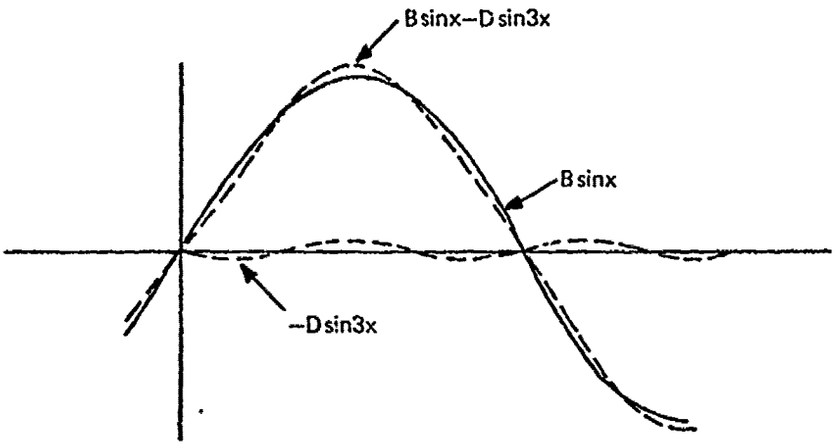

Fig. 20. Proper adjustment of third-harmonic component.

Finally, the third harmonic component must be balanced. The third harmonic mechanism that is being added to the system does not have quite the same mass as the Z-crank hub previously used. Hence, there will also be small changes required in the first harmonic balance. At the point where the scan is as linear as possible we must balance both the first and third harmonic components. It is thu a threefold problem that can be solved if systematically attacked.

Measurement of Scan Error

The scan motion is built to produce a line-of-sight movement that is approximately linear across a 22° field as a function of time. It should ideally produce no vertical displacement of the line of sight whatsoever as it is moved horizontally through the 22° arc.

Measurement of the scanning error could be done by locating the entire experiment on a single concrete or steel I-beam base, including the target and measuring collimators. The required collimator and target precision can be computed as follows.

In order to check the scan error to 3 arc sec, the accuracy of the experimental measurement in each of the four focal planes would have to be

$$91 \text{ cm} \times 3 \text{ arc sec} \cong 1.35 \times 10^{-3} \text{ cm}$$

where

$$3 \text{ arc sec} \cong 1.5 \times 10^{-5} \text{ rad.}$$

This measurement must be referred back at each point to the angular position of the Z-crank.

One can make a simple experimental setup to measure the vertical deviation using the constant deviation property of a right-angle prism. The right-angle prism, a two-sided corner, reflects light coming into the corner in a horizontal plane throughout a deviation of 180°, no matter what the direction from which it is received (see Fig. 21a). At the same time in the vertical plane, the direction in which the edges are aligned, it is as sensitive to angular displacement as a plane mirror would be in the same position, Fig. 21b. Using this property, one can make an experimental setup to check the vertical displacement of the line-of-sight arc, as shown in Figs. 22a and 22b.

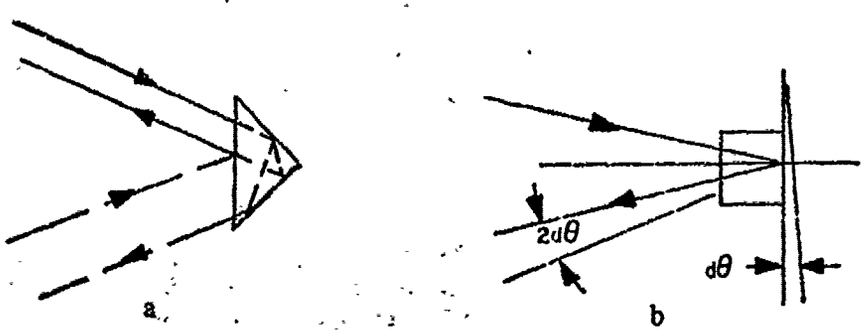

Fig. 21. Properties of a right-angle prism.
a. Horizontal plane.
b. Vertical plane.

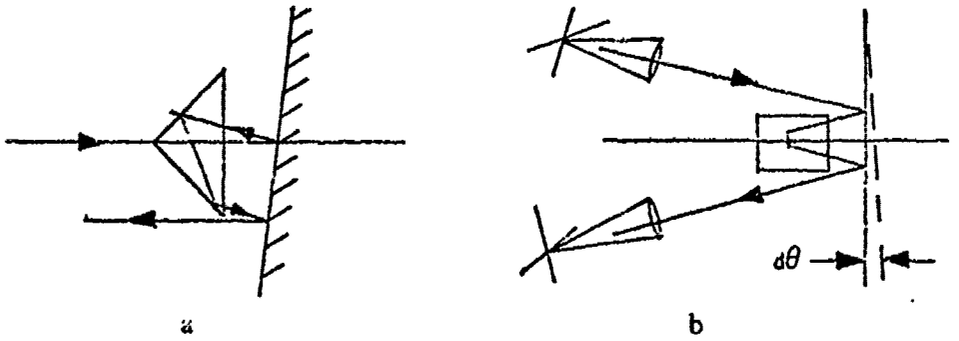

Fig. 22. Experimental setup to measure vertical displacement.

In Figs. 22a and 22b a two-sided corner is shown set up, independent from the Z-crank mirror and with the edges vertical. A plane mirror is affixed to the dummy mirror face on the Z-crank. The collimated target is projected into the system and received with another telescope equipped with a fiducial reticle. Vertical errors will appear as the mirror oscillates through its horizontal scan. This experiment could conceivably be performed with one autocollimator and an illuminated reticle. However, that kind of setup would require a larger prism aperture.

The Space-Worthy Model

The oscillating/rotating mirror design is intended for long-term continuous operation in space. Bearings and gears must be lubricated to provide trouble-free operation in such applications. There is the further consideration that lubricants, if used and exposed to space, must be prevented from diffusing onto the nearby optical surfaces. Consequently, bearings and gears must be either sealed, eliminated, or made to operate in a hard vacuum.

It appears at this moment that in the space-worthy model Z-crank scanner, the A axis and B axis bearings can be replaced by flex joints and the C axis or crank axis, bearings, gears, and weights can be used. Assuming a good seal, nothing will diffuse to the outside to interfere with the optical surfaces in any way. In Fig. 23 the design is indicated schematically.

The A axis is supported by two flex joints, top and bottom, each comprising a pair of split tubes that are installed prestressed in such a way that their natural spring actions tend to cancel each other out. This design is suggested now because at this point we believe that the spring constants should be chosen to eliminate relevant system resonant speeds about the AA' axis. In the same way, the two bearings that now exist on the BB' axis are each to be replaced by a pair of prestressed flex joints.

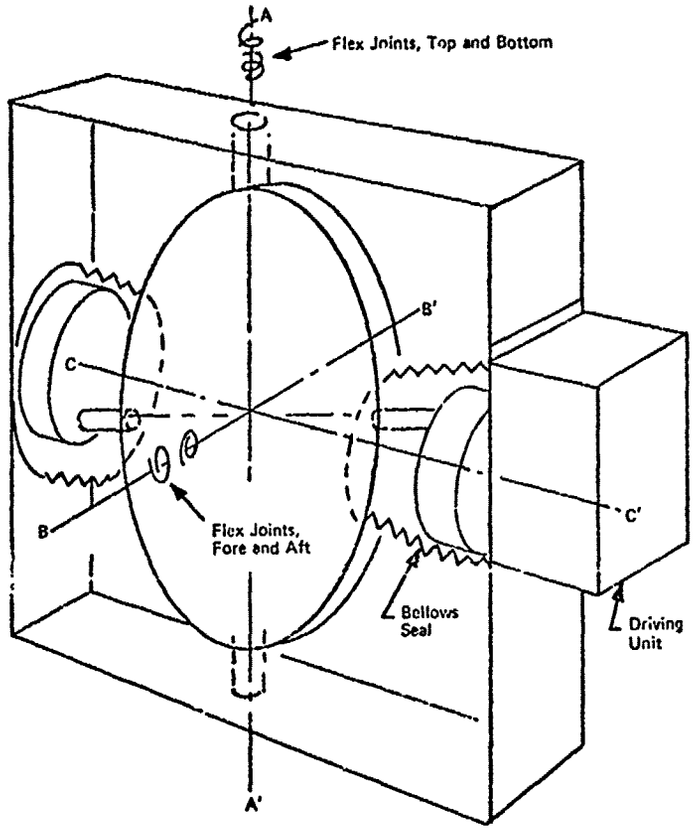

Fig. 23. Space-worthy model of Z-crank scanner.

The CC' axis in the 45-cm model contains the balance weights, the third harmonic mechanism, and a continuous crank traversing the mirror from one side to the other. In considering the sealing of this mechanism, it is necessary to realize two points. First the crank traversing the mirror need not be continuous. Two stub shafts from the crank end to the mirror rim would serve just as well as a continuous shaft. The crank portion shown dotted in Fig. 23 can be eliminated. The second fact that makes sealing possible is that the mirror rim performs only a relatively small quasicircular excursion in response to the stub shaft driving action. Thus, a bellows seal can be devised that is a boot extending from the frame over the mechanism to the mirror and including the mirror stub shaft bearing. On the other side of the frame another bellows seal will enclose the first harmonic balance weight and the drive motor. Flexible bellows can be purchased in a large variety of sizes, some of which have been tested to greater than 2.5×10^8 flexures without leakage. The present problem requires 2×10^8 flexures in a three-year time period. This application therefore is within the present art.

IV. OPTICS FOR OBJECT-PLANE SCANNERS

The six object-plane scanning systems discussed above all lie in front of *and are separate from* the imaging system. They all generate a line scan pattern that can be used in conjunction with a linear array of detectors. Therefore, the instantaneous field of view of the imaging system is a one-dimensional, 22° field. We have not yet considered in detail the problems involved in designing an $f/3.5$, 22° system with a 1-m effective aperture that has a resolution of 3 arc sec; however, we realize that these specifications are pushing the state of the art. The classical curved-field Schmidt is probably the simplest optical system that has a possibility of yielding satisfactory performance.

Standard Schmidt

In the standard Schmidt system the stop and an aspheric corrector plate are located at the center of curvature of a spherical primary. A scanning mirror could be placed in front of the corrector plate as shown in Fig. 24.

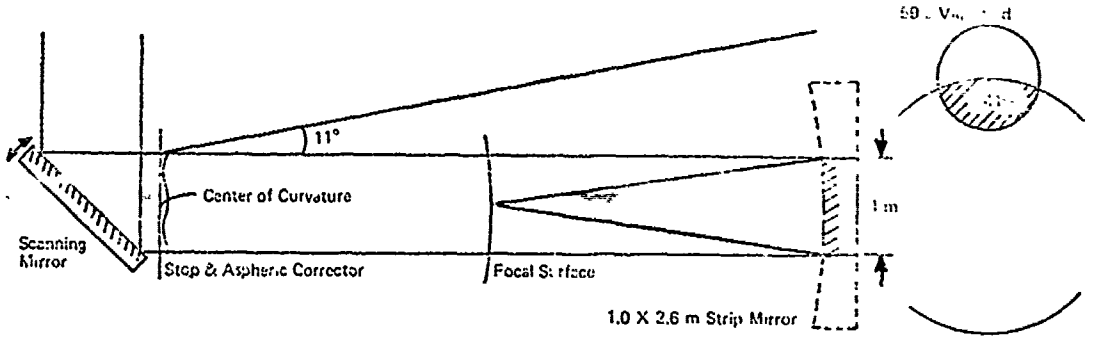

Fig. 24. Standard Schmidt system.

The location of the stop determines the size of the primary mirror and the scanning mirror. For a one-dimensional field, the primary need be only 1 m wide in one direction; however, increasing the size of the primary to 2.6 m in the other direction still results in 59% vignetting at the edge of the 22° field. The scanning mirror would have to be at least 1.5 m in diameter. Furthermore, the system is greater than 7 m in length and the image plane obstructs the incident beam.

Modified Schmidt

There are several ways in which the standard Schmidt system can be modified by moving the location of the stop and scanning mirror with respect to the center of curvature of the primary mirror.

If the stop position is moved to minimize the size of the scanning mirror, then the primary mirror must be increased in size or the vignetting will become even worse.

If the Schmidt system is folded by placing the scanning mirror between the aspheric corrector and the focal surface, the vignetting can be reduced, but now the aberrations become intolerable because the aspheric plate is optically moved from its correct position at the center of curvature of the primary mirror.

Refractive Schmidt

If sufficiently large refractive elements can be made with satisfactory transmission at 3 μm, then perhaps a refractive Schmidt system would become feasible. The elements would still be large and the system would be even longer than its reflective analog; however, we would no longer have the problem of the image plane obstructing the incident beam.

Off-Axis Reflective Schmidt

This system incorporates the scanning mirror into the imaging system by doing the scanning with a reflective aspheric element at the center of curvature of the primary mirror, Fig. 25. A serious disadvantage of this design is that the aspheric corrector plate is not rotationally symmetric but has elliptical zones that make it difficult to fabricate. Also, even if a perfect corrector were made, rotating it by the necessary 5.5° to obtain the scan motion would cause significant aberrations. The severity of this effect will have to be calculated.

This design requires one entire side of the system envelope to be open.

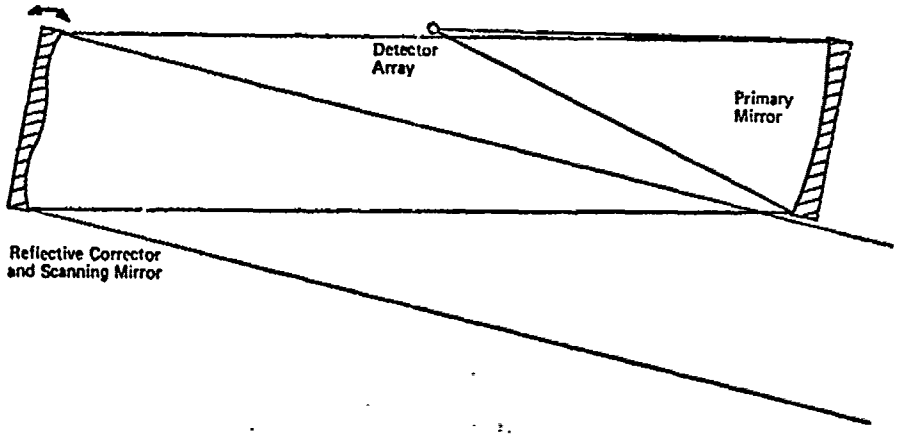

Fig. 25. Off-axis reflective Schmidt.

Off-Axis Doubly Reflective Schmidt

Several possible modifications of the above system can be made by inserting another mirror. The scanning could be done with the new mirror thus allowing the aspheric corrector mirror to remain stationary. Or two aspherics could be used to try to control the aberrations. The use of two mirrors eliminates the need to have one entire side of the system envelope open. Various geometries could be compared to obtain the optimum configuration.

V. OBJECT-PLANE SCANNING WITH TWO-DIMENSIONAL SCAN PATTERN

Risley Prism Scan Patterns

In view of the difficulties encountered on trying to obtain satisfactory imagery over a 22° field of view, it should be noted that the family of scanning mechanisms related to the Risley prisms can generate a variety of two-dimensional scan patterns including spirals and rosette patterns (see Appendix II). If a two-dimensional scan pattern were used, the field over which good imagery must be obtained might be reduced considerably. This would be accompanied by a corresponding reduction in the number of detectors required to span the field. However, for spirals and rosettes, the detector array would have to rotate in the image plane to satisfactorily cover the object field.

Lissajous Figure Scan Patterns

Another family of curves known as Lissajous figures forms a set of possible scan patterns that can be easily generated by oscillating or rotating mirrors or prisms.

The parametric equations describing these curves are

$$x = A_1 \cos(\omega_1 t + \phi_1)$$

$$y = A_2 \cos(\omega_2 t + \phi_2).$$

Four possible Lissajous figure scan patterns are illustrated in Fig. 26. Three scanning mechanisms capable of generating Lissajous figure scan patterns are shown in Fig. 27. The scanning mechanism of Fig. 27a has the advantage of being a straight-through, unfolded system with no net torques or momenta; however, it has a serious materials problem and would also be extremely heavy.

Figure 27b shows an all-reflective system consisting of two oscillating mirrors. This system has uncompensated momenta, and the mirrors experience accelerations that tend to deform the mirror surface. These arrangements are generalizations of the sinusoidal scans discussed in the section on object-plane scanning systems.

The system illustrated in Fig. 27c consists of four mirrors rotating about axes at a small angle to the mirror normal. Each mirror therefore wobbles and sweeps out a circular pattern. This system is all-reflective and has no uncompensated momenta; however, it has a rather large volume and weight.

The Lissajous figure scan pattern, although easy to generate, does not satisfy the requirement that the scan velocity be constant across the field of view.

Linearized Lissajous Figure Scan Patterns

A Z-crank scanning mechanism that is completely balanced and requires only a constant driving torque has been shown to be capable of providing constant scan velocity (within ±1%) over 70% of the scan, the rest being used as turnaround time. This is achieved by introducing into the driving mechanism a small amount of the third harmonic of the fundamental driving frequency.

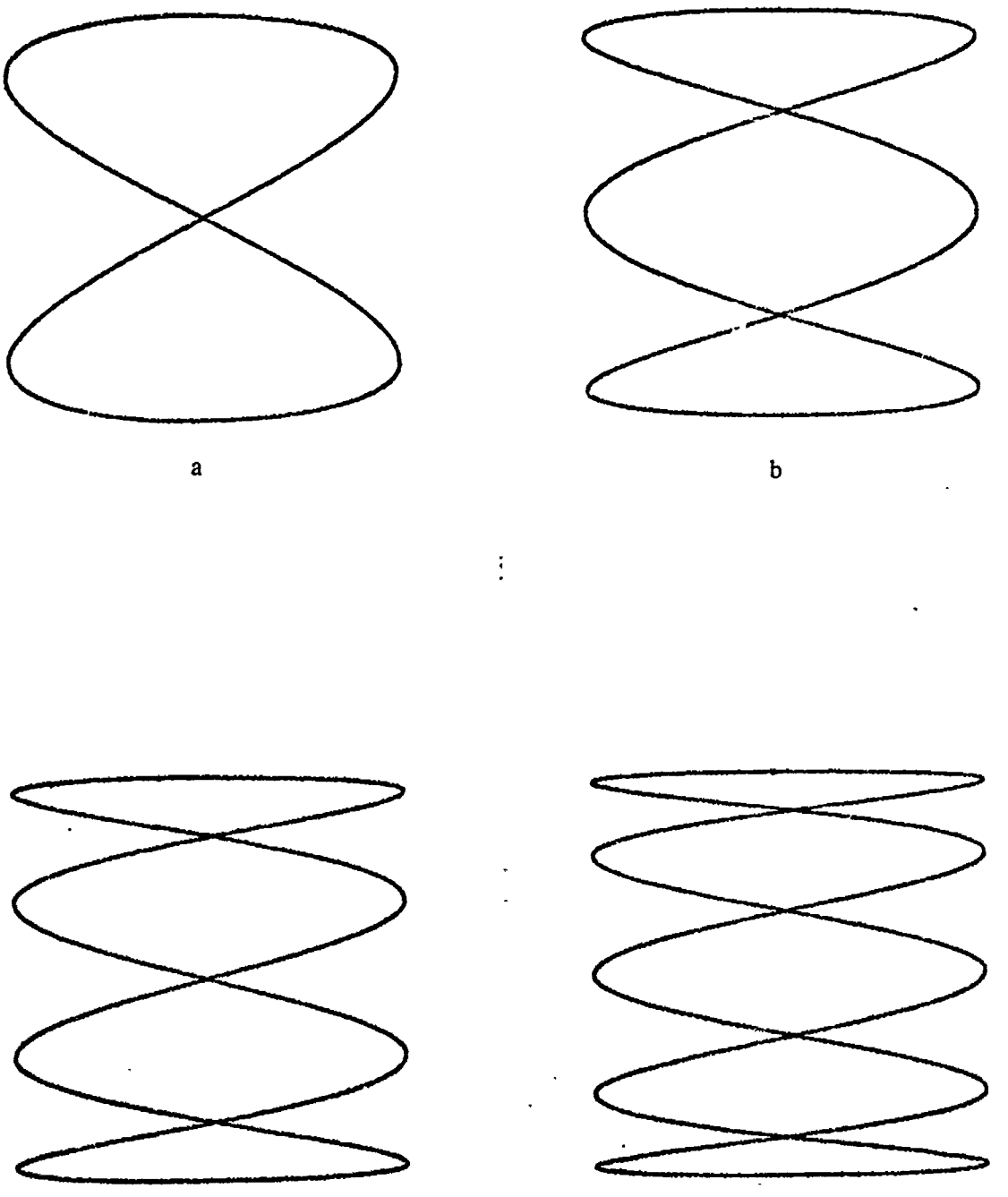

Fig. 26. Lissajous figure scan patterns.
a. $\omega_2/\omega_1 = 2$.
b. $\omega_2/\omega_1 = 3$.
c. $\omega_2/\omega_1 = 4$.
d. $\omega_2/\omega_1 = 5$.

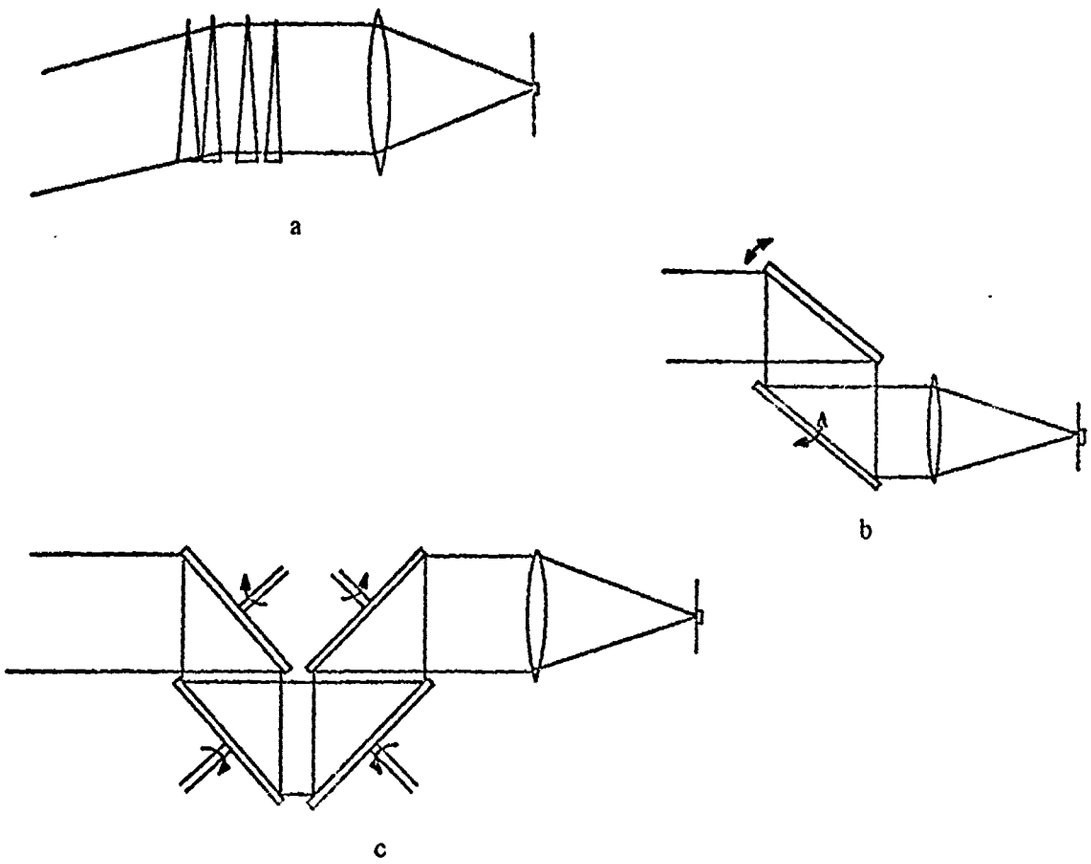

Fig. 27. Scanning mechanisms for generating Lissajous figure scan patterns.
a. Two pairs of Risley prisms.
b. Two oscillating mirrors.
c. Four rotating (with wobble) mirrors.

Two of these units could be used in the configuration of Fig. 27b to provide a two-dimensional scan pattern. The parametric equations describing the family of possible curves are

$$\theta_x(t) = A_1 \cos(\omega_1 t + \phi_1) + B_1 \cos(3\omega_1 t + \delta_1)$$

$$\theta_y(t) = A_2 \cos(\omega_2 t + \phi_2) + B_2 \cos(3\omega_2 t + \delta_2).$$

It has been shown that setting $B_1/A_1 = B_2/A_2 = 0.068$, $\delta_1 = 3\phi_1$, and $\delta_2 = 3\phi_2$ will result in each component of the scan velocity being constant to within ±1% over 70% of the total scan. The additional requirement that $A_1 = B_1$, $\phi_1 = -\pi/2$, and $\phi_2 = 0$ yields

$$\theta_x(t) = A_1 [\sin(\omega_1 t) - 0.068 \sin(3\omega_1 t)]$$

$$\theta_y(t) = A_1 [\cos(\omega_2 t) + 0.068 \cos(3\omega_2 t)].$$

Several possible scan patterns are shown in Fig. 28. Only that portion of the curve enclosed in the dotted box satisfies the linearity requirement. We thus see that $0.7(1.068A_1) = A/2$, where A is the angular field diameter over which constant scan velocity is obtained. Therefore,

$$\theta_x(t) = (A/1.5)[\sin(\omega_1 t) - 0.068 \sin(3\omega_1 t)]$$

$$\theta_y(t) = (A/1.5)[\cos(\omega_2 t) + 0.068 \cos(3\omega_2 t)].$$

The response time required of the detectors is given by

$$\tau \leqslant \beta/\dot{\theta}$$

where

β = angular resolution

$\dot{\theta}$ = angular scan velocity $= (\dot{\theta}_x^2 + \dot{\theta}_y^2)^{1/2}$.

Differentiating the above equations, we now have

$$\dot{\theta}_x(t) = (A\omega_1/1.5)[\cos(\omega_1 t) - 0.204 \cos(3\omega_1 t)]$$

$$\dot{\theta}_y(t) = (A\omega_2/1.5([-\sin(\omega_2 t) - 0.204 \sin(3\omega_2 t)].$$

Setting $\omega_1 t = 0$, and $\omega_2 t = -\pi/2$, we have

$$\dot{\theta}_x = 0.531 A\omega_1$$

$$\dot{\theta}_y = 0.531 A\omega_2.$$

Therefore

$$\dot{\theta} = (\dot{\theta}_x^2 + \dot{\theta}_y^2)^{1/2} = 0.531 A(\omega_1^2 + \omega_2^2)^{1/2}$$

and

$$\tau \leqslant [1.88\beta/A(\omega_1^2 + \omega_2^2)^{1/2}].$$

Setting $\beta = 3$ arc sec, $A = 22° = 0.384$ rad, and $\omega_1 = 2\pi$ rad/sec, we obtain the following response times required for the various scan patterns.

ω_2/ω_1	τ, μsec
0	$\leqslant$ 11.3
3	$\leqslant$ 3.58
4	$\leqslant$ 2.74
5	$\leqslant$ 2.22

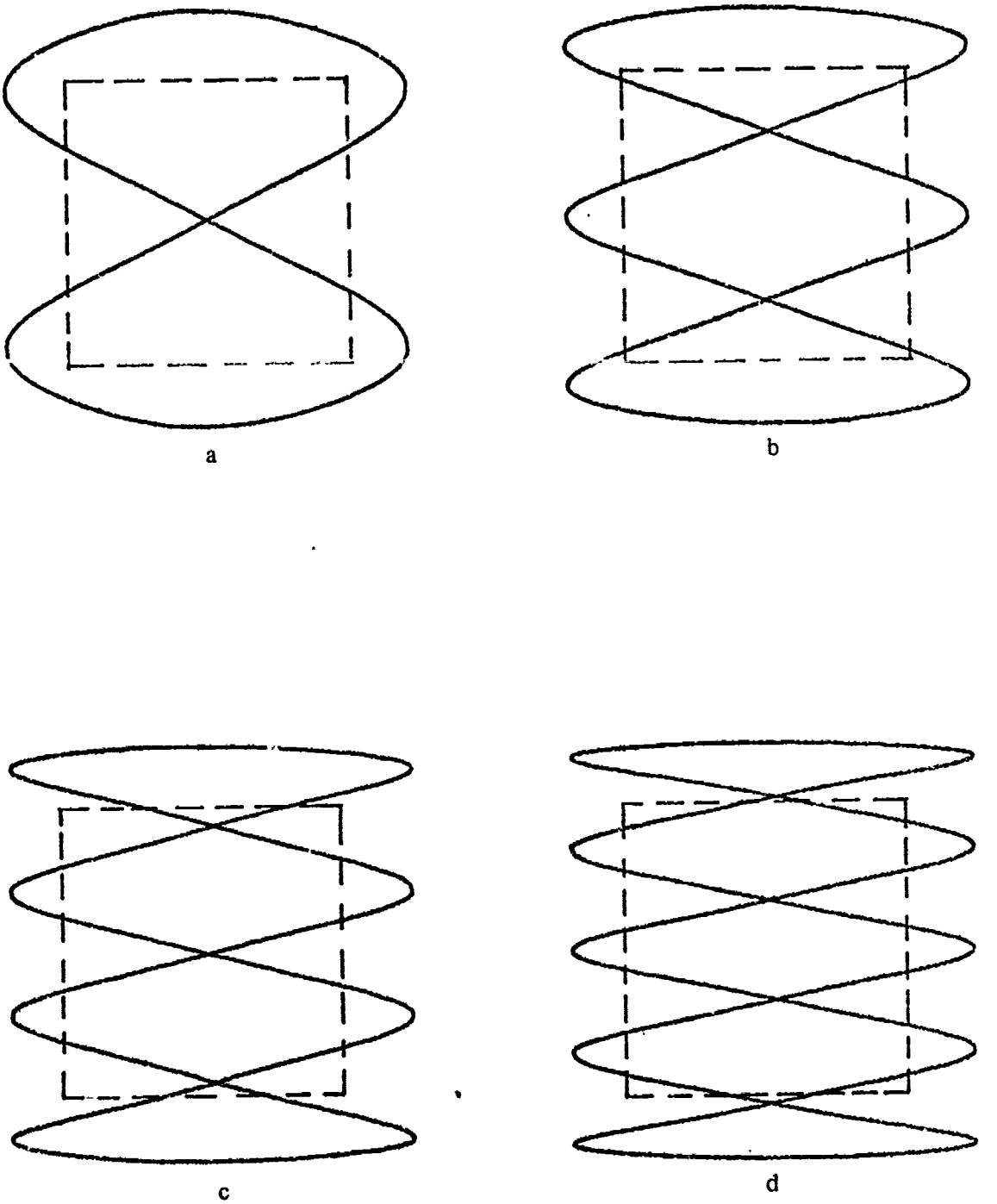

Fig. 28. Linearized Lissajous figure scan patterns.
a. $\omega_2/\omega_1 = 2$.
b. $\omega_2/\omega_1 = 3$.
c. $\omega_2/\omega_1 = 4$.
d. $\omega_2/\omega_1 = 5$.

These are not unreasonable values, as many detectors have response times of approximately 1 μsec.

To calculate the acceleration experienced by the mirrors, we differentiate the angular velocity equations, dividing by two because the mirrors oscillate through only half the scan angle

$$\ddot{\theta}_x(t) = (A\omega_1{}^2/3.0)[-\sin(\omega_1 t) + 0.612\sin(3\omega_1 t)]$$

$$\ddot{\theta}_y(t) = (A\omega_2{}^2/3.0)[-\cos(\omega_2 t) - 0.612\cos(3\omega_2 t)].$$

The maximum angular acceleration for either mirror is thus given by

$$\ddot{\theta}_{max} = 0.538\,A\omega^2.$$

The maximum linear acceleration at the edge of the mirror and expressed in g's is given by

$$\ddot{x}_{max} = r\ddot{\theta}_{max}/g$$

where r is the radius of the mirror and $g = 9.8$ m/sec^2.

Setting $A = 22°$ we can now tabulate the maximum acceleration experienced by mirrors of different sizes oscillating at different frequencies.

ω, rad/sec	$\ddot{\theta}_{max}$, rad/sec^2	$\ddot{x}_{max}$, g's		
		$r = 1$ m	$r = 0.5$ m	$r = 0.167$ m
2π	8.15	0.83	0.42	0.14
6π	73.0	7.44	3.72	1.24
8π	130	13.2	6.60	2.20
10π	201	20.5	10.2	3.40

As some of these accelerations are rather large, it should be pointed out that these maximum accelerations occur during the portion of the scan that is not being used owing to its nonuniform velocity. Hence some elastic deformations can be tolerated at these times so long as the mirror has returned to its proper shape within the time allowed for turnaround.

There is an obvious compromise to be considered in choosing the scan pattern. For the larger values of ω_2/ω_1 the required instantaneous field is smaller as desired; however, the acceleration experienced by the mirror oscillating at ω_2 becomes prohibitively large. This is shown in Figs. 29a, 29b, and 29c.

The scanning efficiency of these patterns is reduced considerably owing to the unused turnaround time during which the scan velocity is not constant, and there is considerable redundancy in covering the desired field of view.

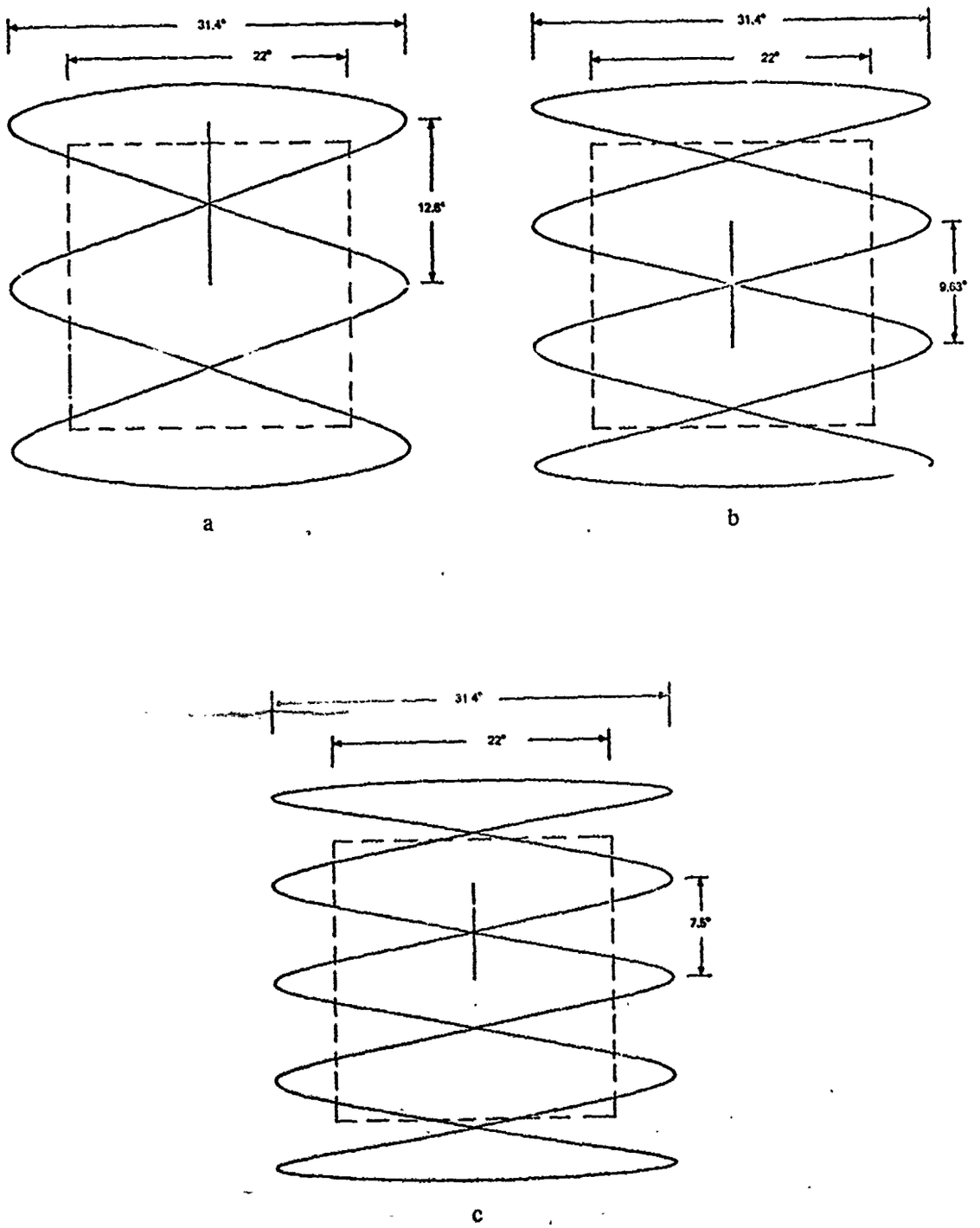

Fig. 29. Instantaneous field of view required of the imaging system for various scan patterns.
a. $\omega_2/\omega_1 = 3$, 12.6° field of view.
b. $\omega_2/\omega_1 = 4$, 9.63° field of view.
c. $\omega_2/\omega_1 = 5$, 7.5° field of view.

VI. CONCLUSIONS

The specifications that a 1-m effective aperture must yield 3 arc sec resolution over a 22° field of view and a scanning time of 1 sec impose severe restrictions upon an infrared system operating at a wavelength of 3 μm.

Provided that 50-μm detectors are available, the system focal length is 3.5 m. This results in an *f*/3.5 cone incident upon the detectors.

Several methods of scanning both the object and image field were investigated and compared. This investigation resulted in the development of two systems that appear to have the desired capabilities: the rotating lens wheel and the oscillating/rotating mirror.

Rotating Lens Wheel

The rotating lens wheel is an image-plane scanning system that yields a linear, unidirectional raster scan with a scan efficiency approaching 100%. Furthermore, there is only one moving part with constant angular momentum that can be easily compensated.

The primary imaging system consists of a stop at the center of curvature of a spherical mirror. The primary image thus suffers only from spherical aberration that is constant over the spherical focal surface. A relay system that corrects the spherical aberration is then pivoted about the center of curvature of the primary image to provide the scan motion.

Sixteen individual relay systems can be appropriately placed on the perimeter of a wheel rotating about the center of curvature of the primary image. This results in an efficient raster scan with 16 lines per frame. The relay system thus has a one-dimensional instantaneous field of view of less than 1.5°. The quality required in the relay systems may allow replicating techniques.

This scanner should be developed further to complete the optical design for the relays consisting of the four mirrors so that their surfaces correct the spherical aberration of the primary and so that the spoke provides adequate resolution over its field. Then one spoke should be constructed and tested. The next step is to make two such spokes and mount them in a wheel to test registration, alignment, resolution, etc. Success along these lines paves the way for constructing a laboratory model of either the 11° or 22° model.

Oscillating/Rotating Mirror

An oscillating/rotating mirror operated by a Z-crank driving mechanism has been developed to the point of being completely balanced and requiring only a constant driving torque while producing a scan velocity that is constant to within ±1% over 70% of the full scan.

Two of these units can be used in an object-plane scanning system to produce a two-dimensional scan pattern. The most suitable imaging system has not been determined, but designing a reflecting optical system with a 7° to 10° one-dimensional field and satisfying the given specifications should be straightforward.

Appendix. I. CONFIGURATIONS FOR A LARGE-FIELD OPTICAL SYSTEM

This appendix concerns the requirement for a system defined by a detector size of 50 μm and a resolution of 3 arc sec. Although there are conflicting interpretations of "resolution" and "detector" size, we will assume that the 50 μm and the 3 arc sec specifications do define the effective focal length, which we compute to be 345 cm. Energy requirements are for a 1.0-m equivalent aperture. The field of view must be at least 22°. The wavelength at which the system operates is 2.7 μm, and filters limit the spectral interval to a relatively narrow band about this wavelength.

Refractive systems can be immediately excluded as too heavy and not amenable to this wavelength. Thin refractive elements such as aspheric correctors can be considered, but here size is important since fused silica is not presently available in large sizes with low enough water content to have high transmission at 2.7 μm. Because the matrix of designs is so limited in meeting the above specifications, we will consider the thin-plate catadioptric systems. One avenue of reaching the desired system might be a major effort to manufacture large thin plates of water-free fused quartz.

Two basic reflective configurations can be considered: prime focus in which the focal plane is essentially inside the system and in the optical beam, and Cassegrain focus in which the focal plane is behind the primary mirror and hence out of the optical beam.

The severest restraint on acceptable mechanical and optical designs is the wide field at an effective $f/3.5$. The field of 22° and focal length of 345 cm means that the diameter of the desired field is 130 cm, which is larger than the desired nominal aperture. As a result the detectors spread entirely across the beam in the prime focus configurations, or the secondary mirror in the Cassegrain focus completely blocks the optical beam. Aside from this purely mechanical problem the high resultant system speed (f-ratio) and wide field stress the available designs since a single aspheric is inadequate for the desired resolution. We will look at both all-reflective configurations and catadioptric ones. The latter are more likely to meet the requirements, with the exception of the transmissibility question.

Scanning Options

The question of optical design is closely coupled to the question of how we are to scan the field with the detectors. Basically we can use a mirror scan where we reflect the optical beam to the detector array, or we can use a detector scan where the optical field is fixed and the detector array moves over the field. The amount of scan by either method is also important to the design because of the angles involved. If a single linear array of detectors is used, either curved to the focal surface or straight, depending on the field curvature of the optical system, then the scanning mirror must move at least ±5.5°. This amount is large enough that one must limit the amount of optical figure that can be placed on the scanning mirror. If several detector arrays span the field, then the angle of scan can be reduced, but one soon gets a system with 40,000 to 60,000 elements, stressing other parts of the system. If we choose the detector scan, then we face microelectronic problems and cryogenic complications, but we do have important options with detector scan systems, so we will discuss some options.

The mode of scanning has other consequences on the system design. The proposed scan time for the 22° field is 1 sec as the maximum allowable rate. The angular accelerations to the structures involved are high and the momentum changes are quite sizable owing to the dimensions and masses involved. Such perturbations to a large optical system can be serious

even though we have what looks at first like a generous image tolerance, 3 arc sec. The optical designer wants the full tolerance (and he may need it for this *f*-ratio and field size) and the structural engineer wants it for lightening the weight of the scanning mirror. For example, one would be tempted to use a thin beryllium disk for the flat, but the allowable error could be absorbed by this one decision.

It may be that a detector scan will involve the minimum mass of moving structure. We would like to see whether the gains in the system design are enough to offset some of the unknowns in the area of solid-state detector array technology.

The basic impact of differences in detector vs mirror scanning is in regard to the shape of the optical elements. The mirror scan method reduces the configuration problem to a one-dimensional field, and mirrors tend to become rectangular sections rather than circular ones.

Catadioptric Configurations

One-Aspheric Schmidt

In view of the basic requirements, the classical curved-field Schmidt is the simplest optical system that has a possibility of yielding satisfactory imagery over the 22° field angle. We soon learn, however, that such a system has practical limitations because of the "diffuseness" of the structure. The stop location, for example, determines the size of the scanning mirror. If we move the stop position to minimize the scanning mirror size, then we have another problem since the size of the primary mirrors changes in the opposite way. Because of enclosure limitations, we are not permitted to use a mirror larger than about 264 cm. If we then minimize the scanning flat, we are faced with the loss of 90% of the light from the extremes of the field, an unacceptable amount.

Figure 1 shows the basic Schmidt configuration. The primary mirror is a strip about 107 cm by 264 cm but has 59% vignetting and a scanning mirror 100 cm in diameter. If we move the stop position as shown in Fig. 2, we require a larger aspheric plate of 130-cm diam. We now have poorer optical aberrations and vignetting of 90%, but the size of the scanning flat is reduced to 119-cm diam. Figure 3 shows the Schmidt folded between the aspheric corrector and the focal surface to improve the vignetting. Although the vignetting is now reduced to about 30%, the optical aberrations become impossible owing to coma since the aspheric plate is optically moved from its correct position at the center of curvature of the primary mirror. The configuration shown in Fig. 1 is the only one that could be considered, and it must be excluded on the basis of off-axis aberrations as well as excessive vignetting.

One-Aspheric Wright

The Wright design looks superficially like the Schmidt except that the aspheric plate is now placed close to the focal surface. In actuality the primary is an ellipsoid, so two aspheric surfaces are required. With two aspherics the design still suffers from aberrations, mainly astigmatism, and the basic design is inadequate for the requirements of this problem.

Three-Aspheric Prime Focus

The least number of aspherics that will correct third-order aberrations is three, in the form of either transmitting plates or reflecting surfaces. The three-aspheric equivalent of a "prime focus" system is shown in Fig. 4. The total system length is now reduced, and the stop is close enough to the primary mirror to reduce vignetting. No scanning flat is shown in Fig. 4

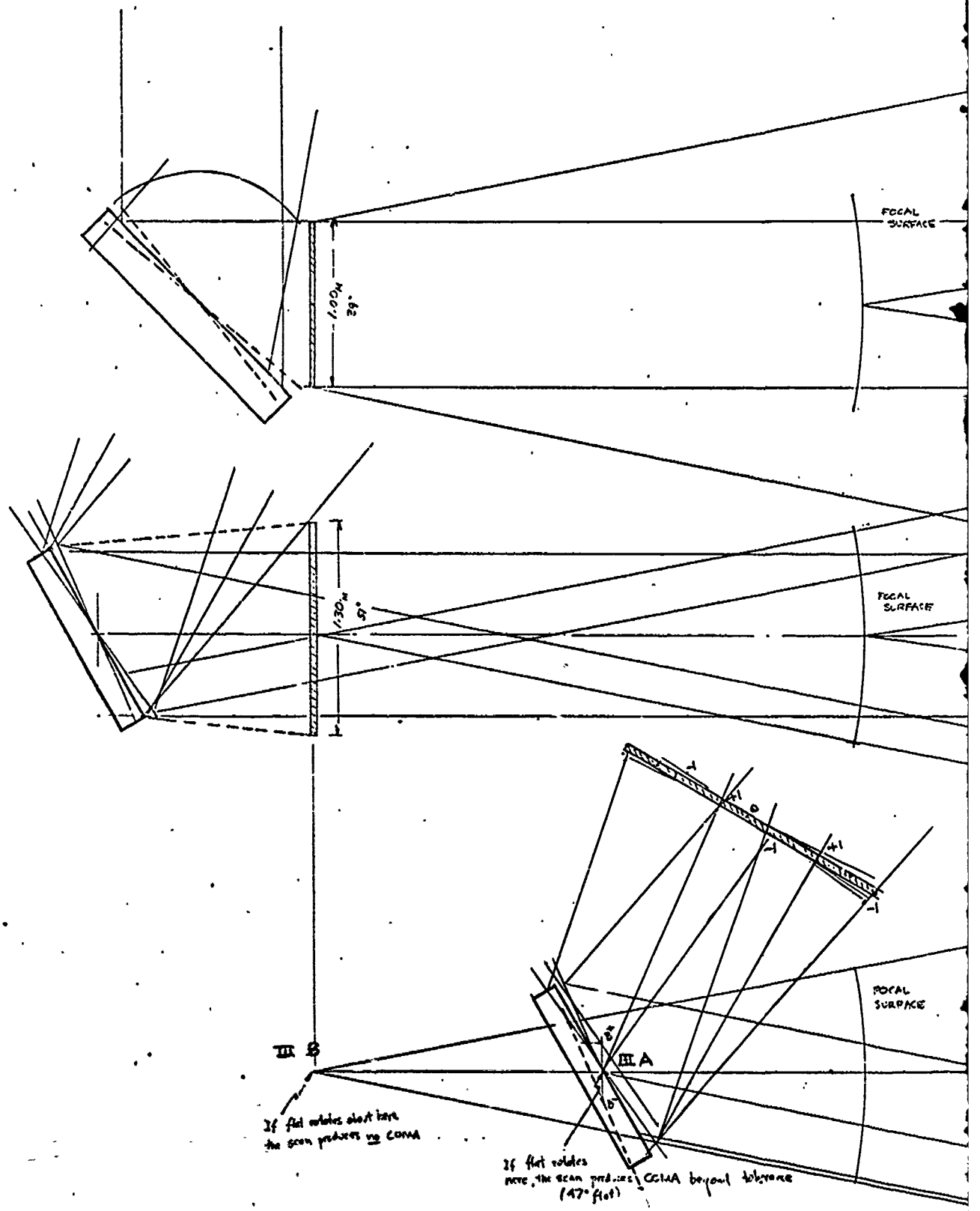
FOCAL SURFACE
FOCAL SURFACE
FOCAL SURFACE
III B
III A
If flat reticles could have the scan produces no COMA
If flat reticles were, the scan produces COMA beyond tolerance (47° flat)

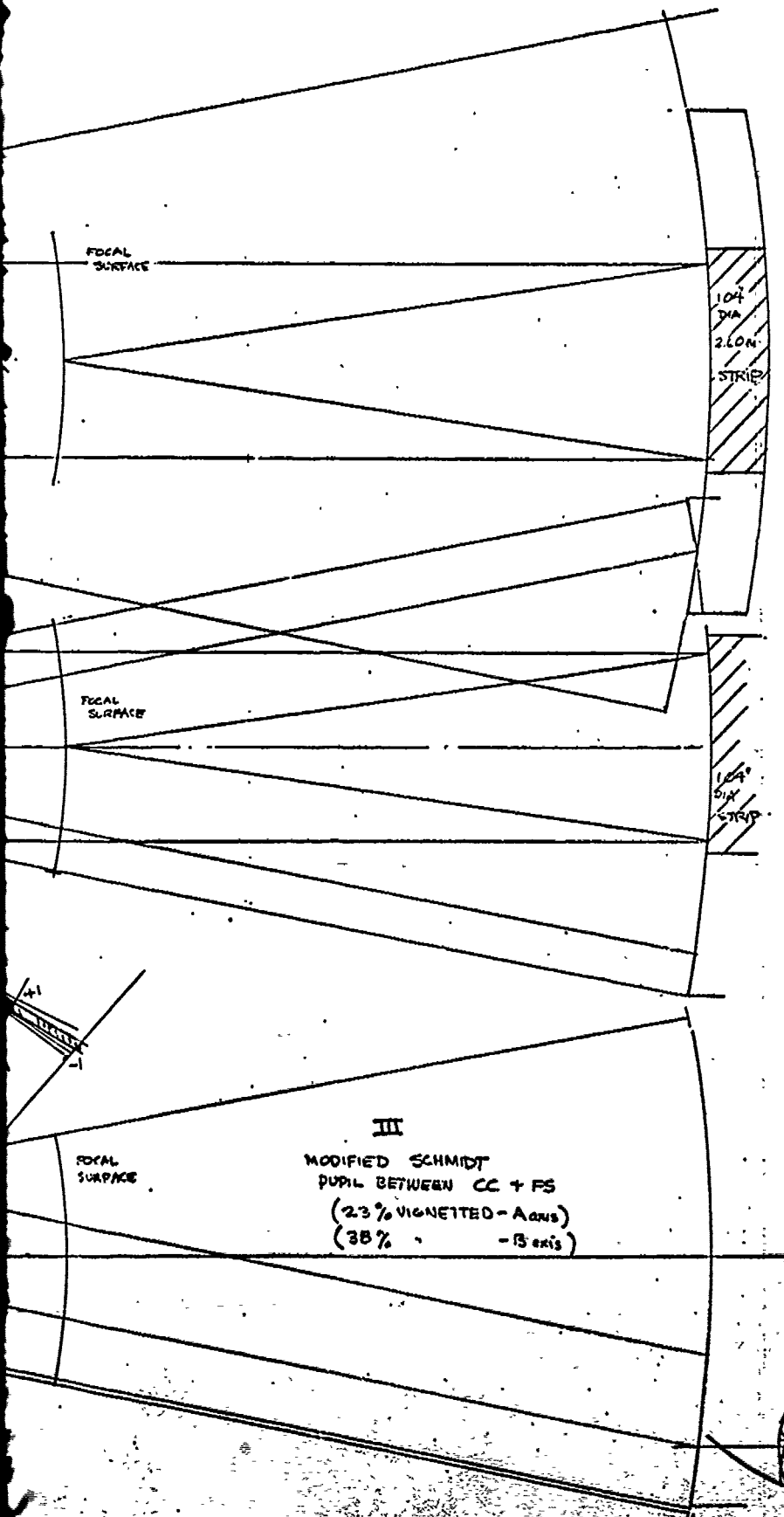

III

MODIFIED SCHMIDT
PUPIL BETWEEN CC + FS
(23% VIGNETTED - A axis)
(38% " - B axis)

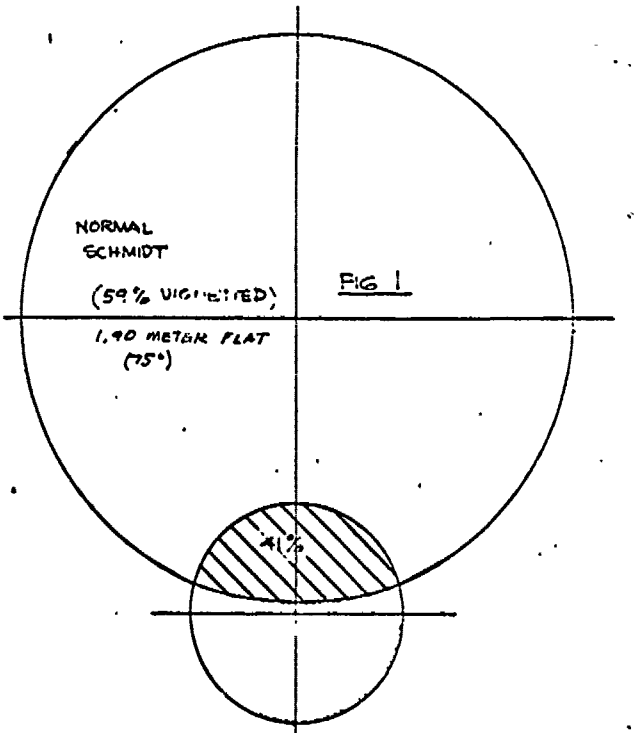

FIG 1

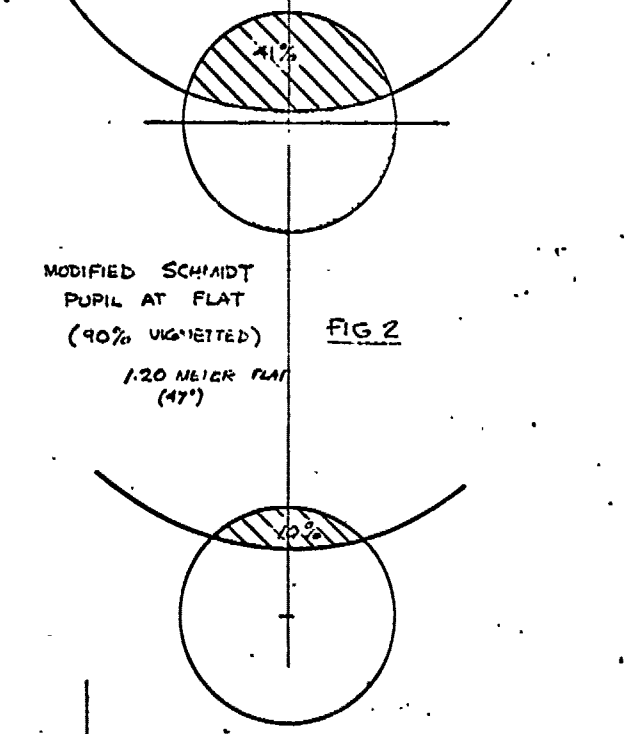

FIG 2

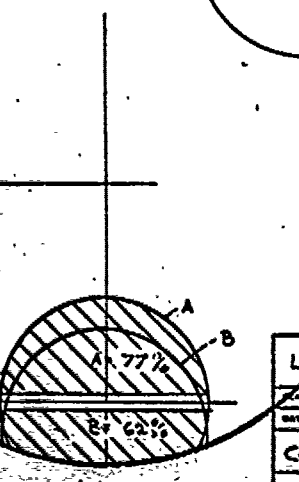

FIG 3

LARGE-FIELD INFRARED SYSTEM	
SCALE 1:2 40 cm	APPD BY
DATE 9 MAR 71	DRAWN BY
COMPARATIVE SCHMIDT DESIGNS	
22° FIELD-MIRROR SCAN	DRAWING NUMBER

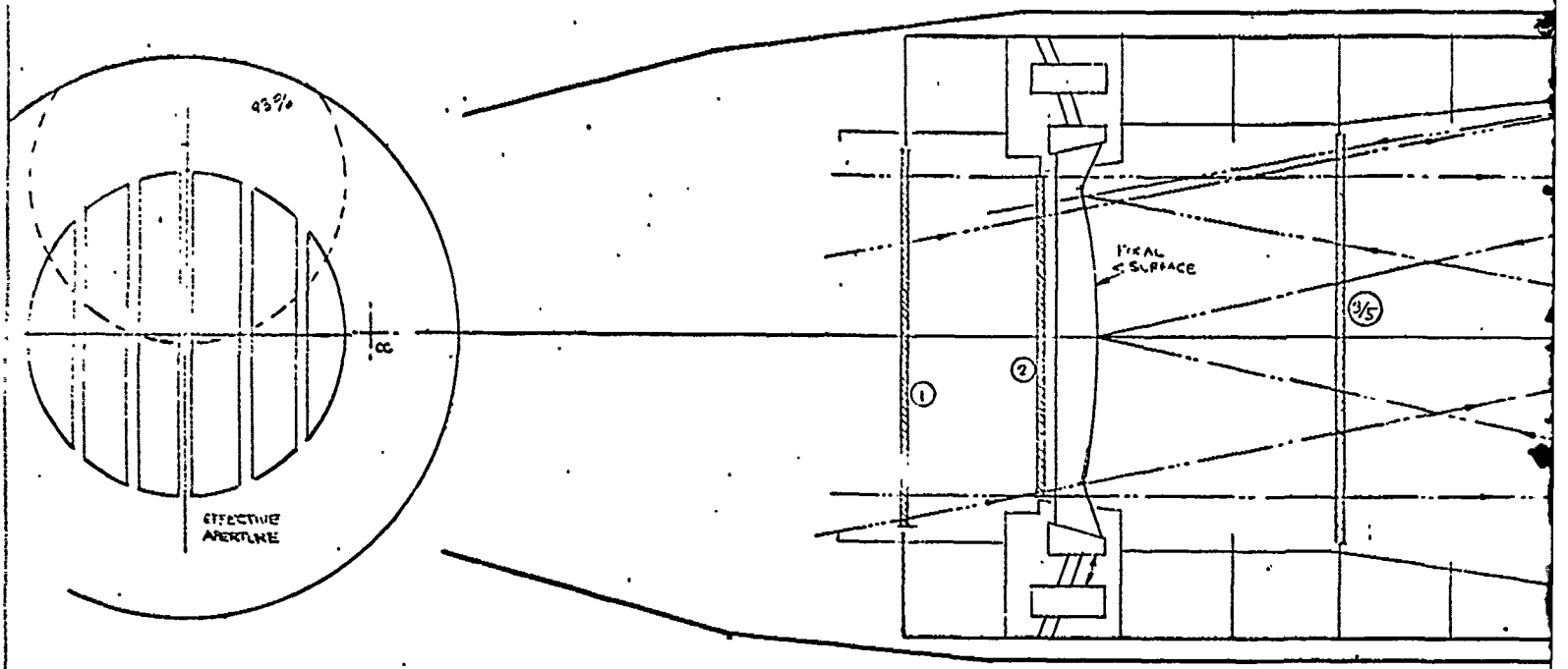
93%
CC
EFFECTIVE APERTURE
FINAL SURFACE
3/5
1
2

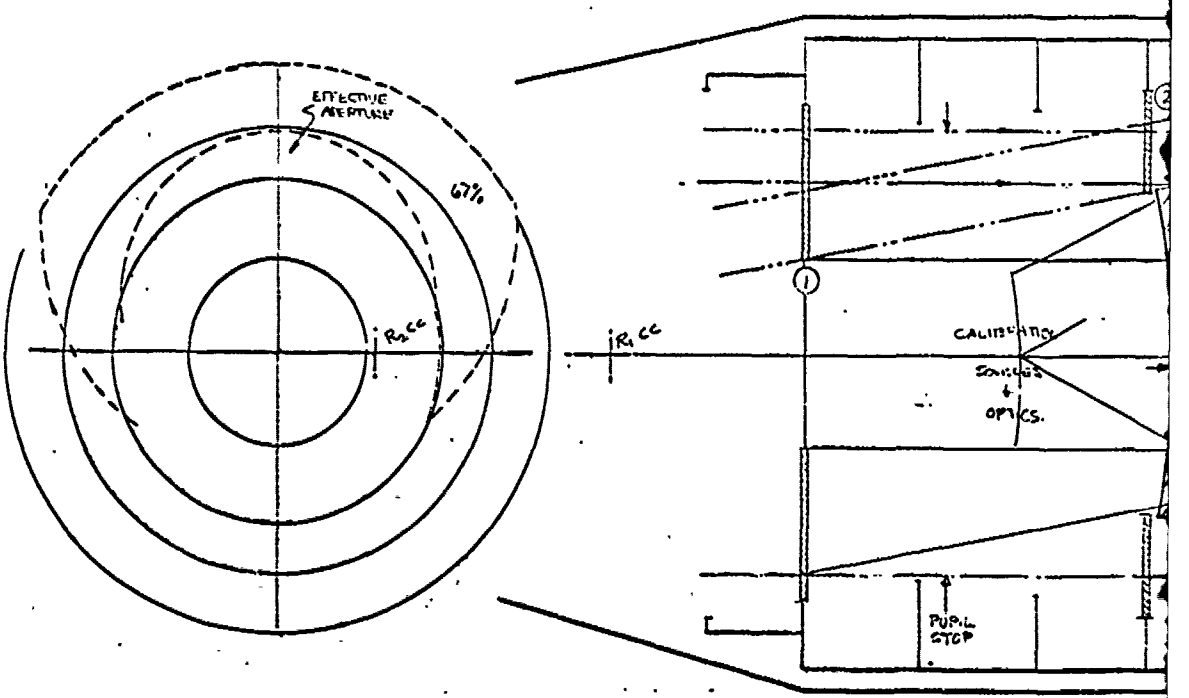
EFFECTIVE APERTURE
67%
R₂CC
R₁CC
CALIBRATION SOURCES & OPTICS
PUPIL STOP
1

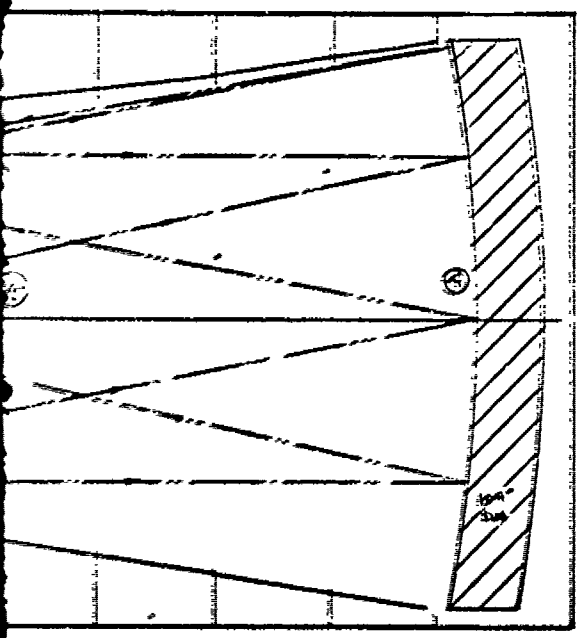

7% VIGNETTING A = 1.35 m²

PRIME FOCUS CONFIGURATIONS

FIG 4

	CASE A	CASE B	CASE C	CASE D
①	A	A	A	—
②	A	A	—	A
③	A	—	A	A
④	S	A	A	A

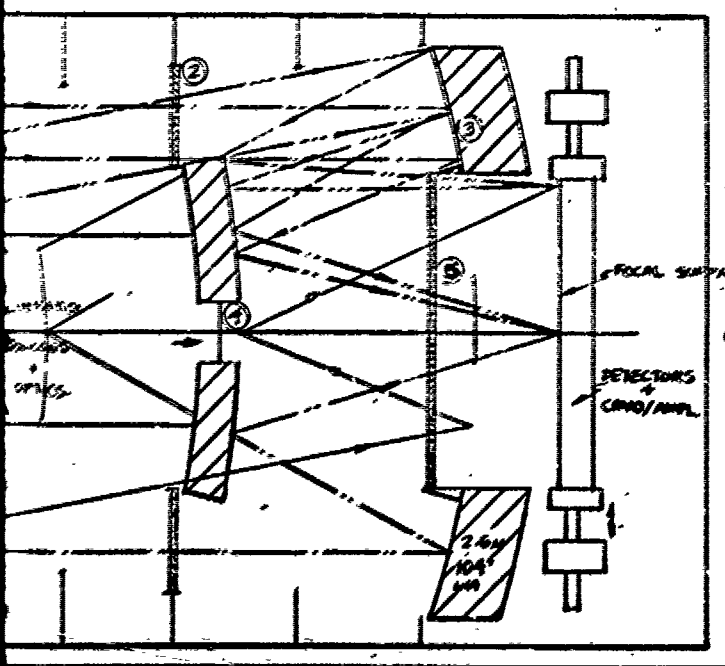

7% VIGNETTING A = 1.00 m²

33% VIGNETTING A = 1.30 m²

CASSEGRAIN CONFIGURATIONS (FLAT FIELD)

FIG 5.

	CASE A	B	C	D	E	F
①	A	—	—	—	A	A
②	A	A	A	A	A	A
③	S	A	S	A	A	S
④	S	S	A	A	S	A
⑤	A	A	A	—	—	—

ULTRA-SHORT SYSTEMS.

LARGE-FIELD INFRARED SYSTEM

COMPARATIVE DESIGNS

22° FIELD-DETECTOR SCAN

since it would be too large to be considered. Figure 4 therefore is applicable only to the case of detector scanning.

The basic three-aspheric prime focus system has a curved field, just like the Schmidt system. A field flattening lens could be added just in front of the focal surface, but weight and optical transmission as well as other considerations indicate that it is not particularly desirable.

Figure 4 shows three thin corrector plates and one mirror. We therefore have four options for distributing the aspheric terms. For example, if we allow the mirror to be aspheric, then one of the transmitting plates could be eliminated. Each design option should be explored to see which option is most easily manufactured and is least sensitive to collimation.

The basic optical aberrations of a three-aspheric system are so much lower than for a Schmidt or Wright that we can increase the light-gathering power of the system by using an aperture that is larger than 1 m in diameter. The design shown in Fig. 4 has approximately twice the energy-gathering capability of those in Figs. 1, 2, and 3. Also the tube length is shorter and the total weight relative to the 264-cm mirror, common to all designs, is reduced significantly.

Three-Aspheric Cassegrain Flat Field

A Cassegrain configuration is desirable because the focal surface occurs outside the optical beam. It can be placed completely behind the primary mirror where systems engineers can fully develop the detector array system without worrying about encroachment on the optical beam. The Cassegrain system, moreover, permits us to flatten the focal surface without using a field flattening lens. Figure 5 shows a flat-field configuration of a very compact nature. We now have quite a few options of how to distribute the asphericity; six are shown in Fig. 5.

The principal problem with finding a satisfactory Cassegrain design is the large linear size of the field of view of 22° and the large secondary mirror. The design shown is unique in that no other geometry will satisfy these conditions and yield sky baffling without excessive vignetting. The main result of this study is that *no* solutions exist unless the aperture of the stop is increased from the original specification of 1 m up to a new diameter of 2 m. The system geometrical *f*-ratio is made twice as fast, *f*/1.75, but again the deployment of three aspherics seems adequate to meet the design specifications for 3-arc-sec images.

No scanning mirror can be used with this configuration because of the prohibitive sizes involved, but there is adequate room to develop a sophisticated detector scan system. The tube length for the Cassegrain system is short, about 381 cm, half that of the Schmidt. If the No. 1 aspheric can be eliminated, the length reduces to about 305 cm. Vignetting is quite small for these designs as shown in Fig. 5.

Three-Aspheric Concentric Cassegrain

One curved-field Cassegrain is of interest because of its relationship to the standard Schmidt geometry. Figure 6 shows a concentric Cassegrain, a two-mirror system with complete symmetry about a single center of curvature. As a consequence the field aberrations are naturally small, and three relatively weak aspheric surfaces can yield excellent optical performance. The field is curved concave. Again, solutions exist only when the aperture stop is 2.0 m in diameter. The concentric Cassegrain is the most compact and, if the No. 1 aspheric

is eliminated as in case B in Fig. 6, the total system length is less than the primary mirror diameter. Vignetting is relatively small for this design when the aspheric plates are oversize as shown and the stop is as indicated.

The three-aspheric concentric Cassegrain must be used in the detector-scan mode because a scanning flat would be prohibitively large. The configuration has two mirrors as shown, but their total weight is less than that of the primary for the Schmidt configuration.

Refractive Schmidt

For the sake of completeness, we show the refractive equivalent of the Schmidt in Fig. 7. The system is surprisingly simple, but the scanning flat or the power element becomes large. If sufficiently large transmitting elements can be made with satisfactory transmission at 2.7 μm, then this elegantly simple design might become of interest.

Reflective Configurations

In view of the problem inherent in the 2.7-μm water vapor absorption in fused silica and fused quartz, it may not be possible to use the thin aspheric plate design solutions discussed above. The general rule that three aspherics will give a satisfactory design applies to reflective surfaces, but we find that it is difficult to arrive at a satisfactory mechanical design when the third mirror is desired. To date we have found only one three-mirror configuration that has desirable properties, but since there is only one single-aspheric reflective design to be considered, we must look at both the single-aspheric and three-mirror designs.

Reflective Schmidt

Figure 8 shows the reflective equivalent of a Schmidt where the reflective corrector is placed at the center of curvature of the primary. The first problem posed by this design is that the aspheric plate is not rotationally symmetric. We must make elliptical zones, and since even high-quality symmetrical aspherics give manufacturing difficulties, the quality to be expected of a nonsymmetrical aspheric can be lower. New manufacturing methods such as ionic polishing need to be explored in the context of new ways to get such aspherics.

A second problem with the reflective Schmidt is that rotation of the aspheric reflector, as would be necessary for mirror scanning, causes optical aberrations, and even a perfect corrector for the on-axis focal position would cause significant aberrations when the mirror is scanned.

The reflective Schmidt has serious vignetting, 60%, and has a system envelope that requires one entire side to be open to accommodate the optical ray bundles over the field of view.

Three-Aspheric Inverted Cassegrain

One possible solution to the three-mirror design is shown in Fig. 9. The basic group consists of two concentric spheres with the convex mirror being No. 1. The resultant focus is far to the left, but a third mirror, a plano aspheric, is used to fold the beam, placing the focus behind the No. 1 mirror. We get a surprisingly good system with relatively weak aspherics on the three mirrors. We cannot use the aspheric plano as a scanning mirror for the same reason it won't give good performance for the reflective Schmidt case—namely, the optical center of the plano aspheric shifts off the system axis and coma is produced.

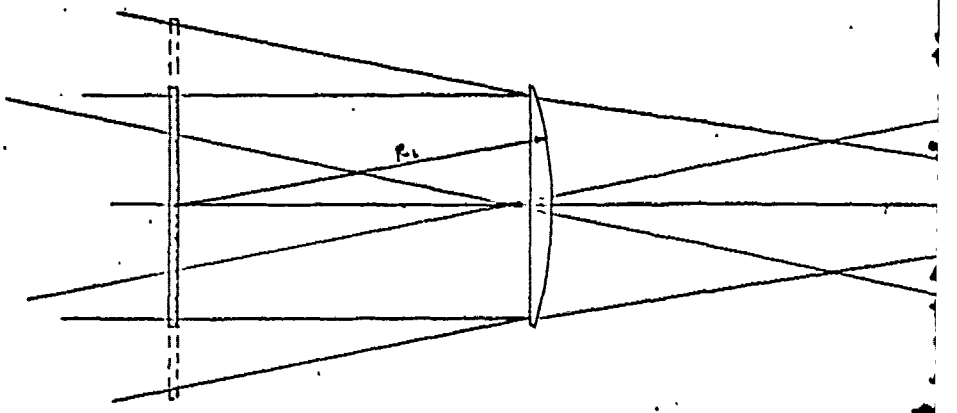

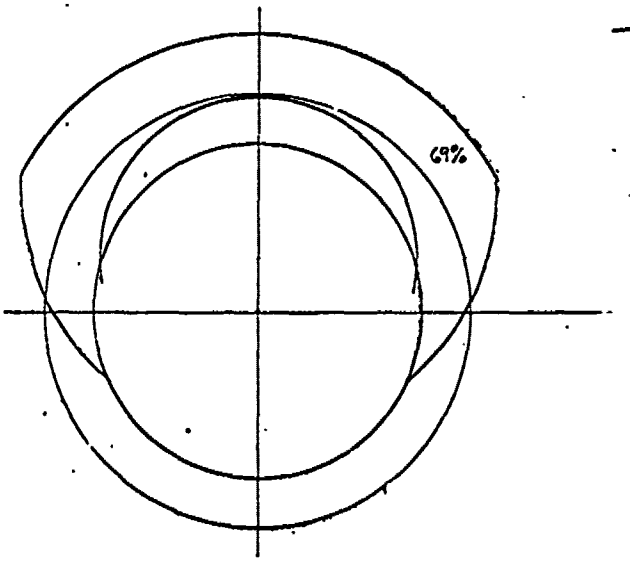
69%

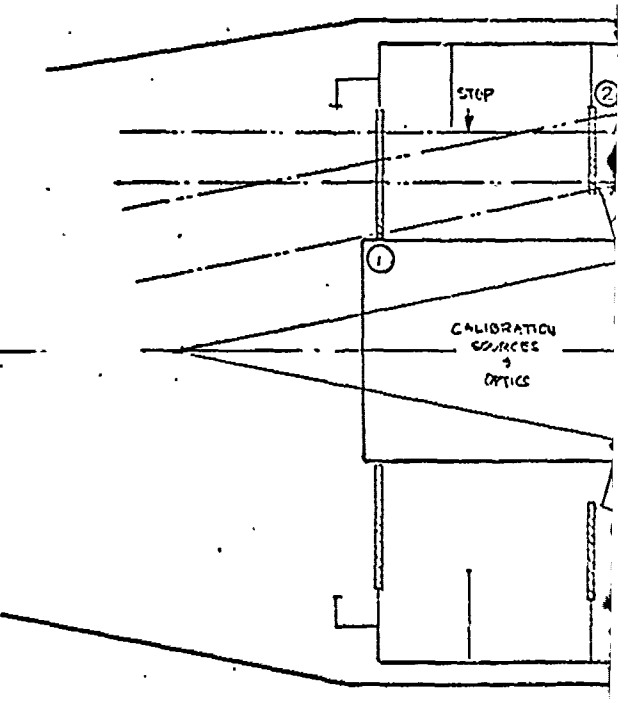
STOP
2
1
CALIBRATION
SOURCES
&
OPTICS

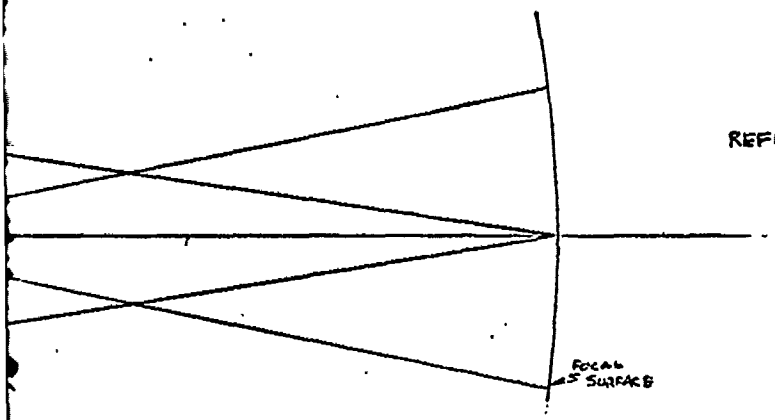

REFRACTIVE SCHMIDT FIGURE 7

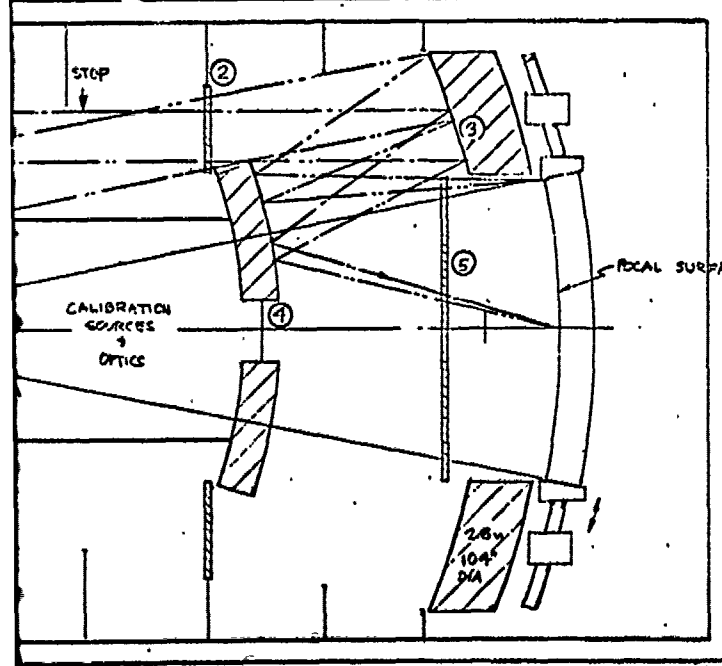

7% VIGNETTING $A = 1.00\ M^2$

31% VIGNETTING $A = 1.30 M^2$

CASSEGRAIN CONCENTRIC (CURVED FIELD) FIGURE 6

CASE	A	B	C	D	E	F
1	A	—	—	—	A	A
2	A	A	A	A	A	A
3	S	A	S	A	A	S
4	S	S	A	A	S	A
5	A	A	A	—	—	—

LARGE-FIELD INFRARED SYSTEM

COMPARATIVE DESIGNS

22° FIELD - DETECTOR SCAN

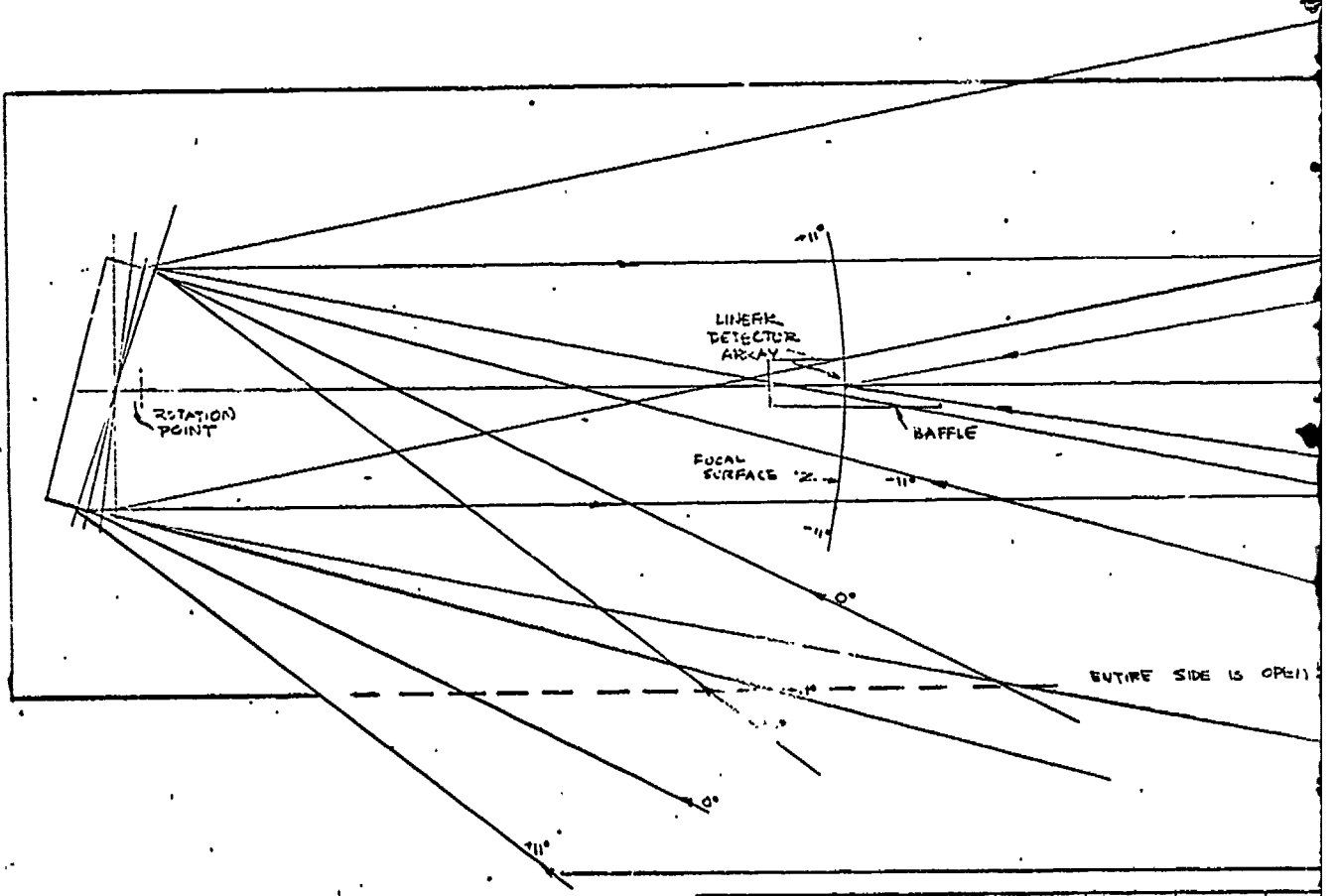
+11°
LINEAR DETECTOR ARRAY
ROTATION POINT
BAFFLE
FOCAL SURFACE "Z"
-11°
-11°
0°
ENTIRE SIDE IS OPEN
0°
+11°

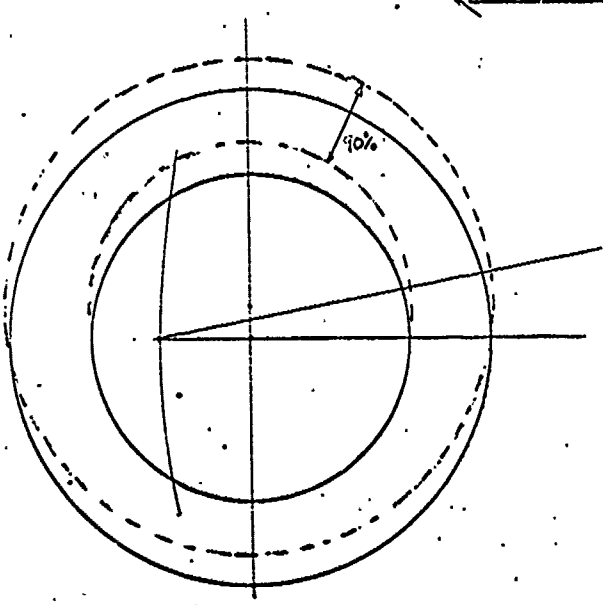
90%

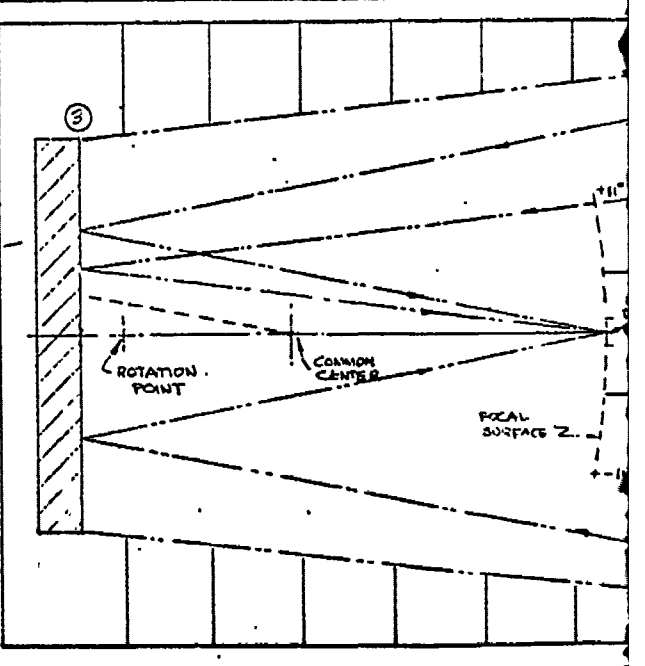
3
+11°
ROTATION POINT
COMMON CENTER
FOCAL SURFACE "Z"

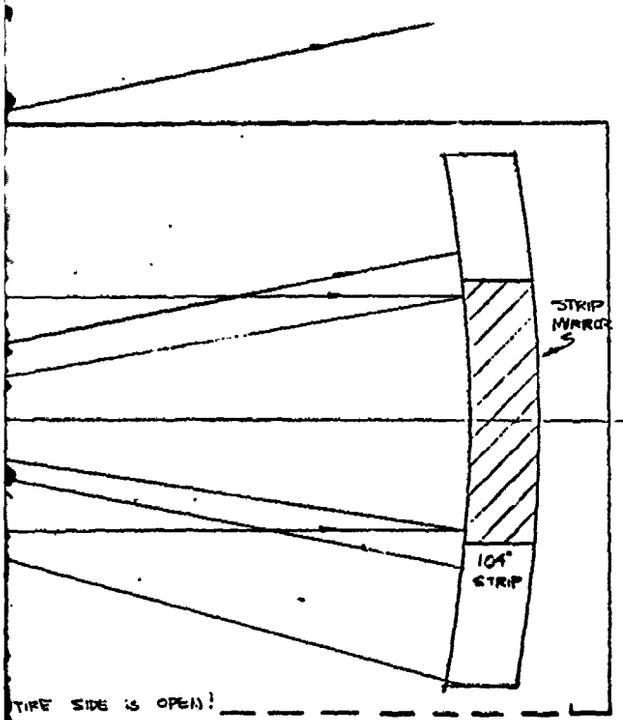

REFLECTIVE SCHMIDT
59% VIGNETTING
(NON-ROTATIONALLY SYMMETRIC ASPHERIC)

FIGURE 8

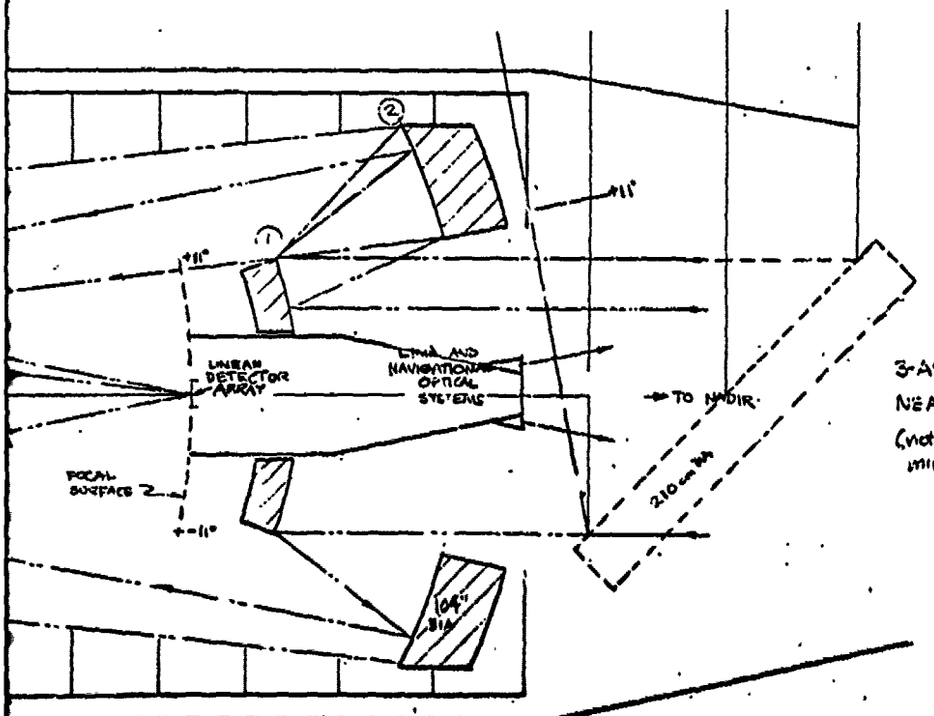

3-ASPHERIC INVERTED CASSEGRAIN
NEAR-CONCENTRIC
(note decentered rotation point to minimize error in # 3 aspheric)
10% VIGNETTING

FIGURE 9

LARGE-FIELD INFRARED SYSTEM		
SCALE: 1" = 40cm	APPROVED BY:	DRAWN BY: AHK
DATE: 5 MAR 71		DRAWING NUMBER
ALL REFLECTIVE SYSTEMS		
22° FIELD-MIRROR SCAN		

FLAT

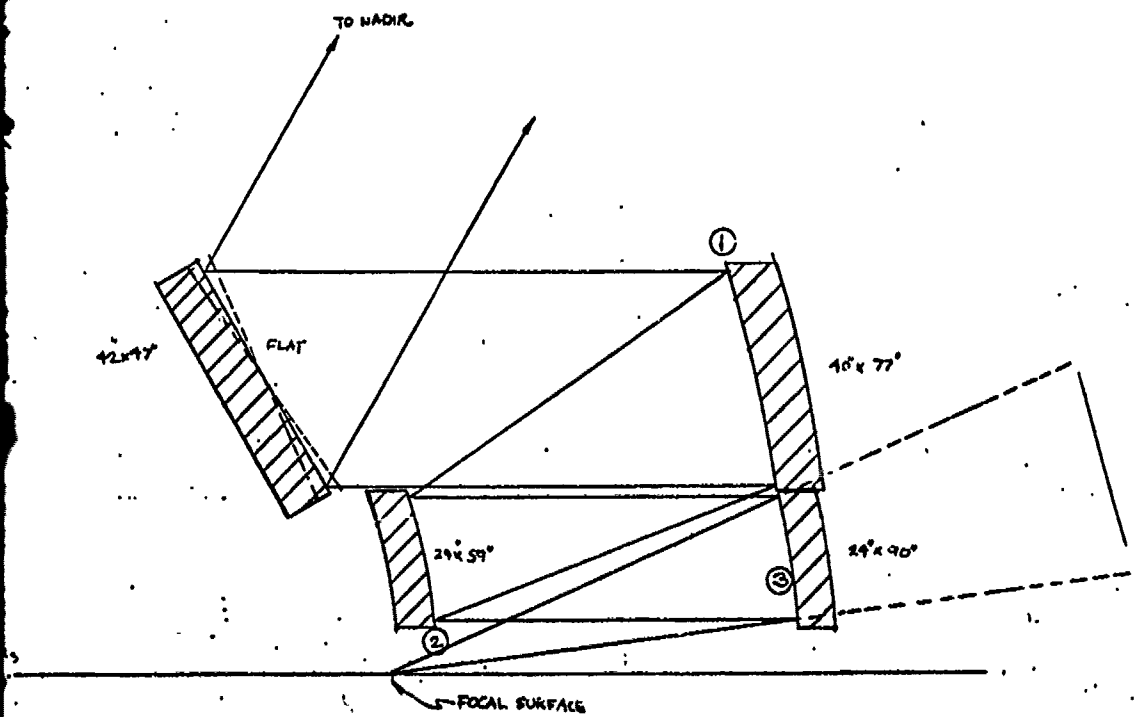

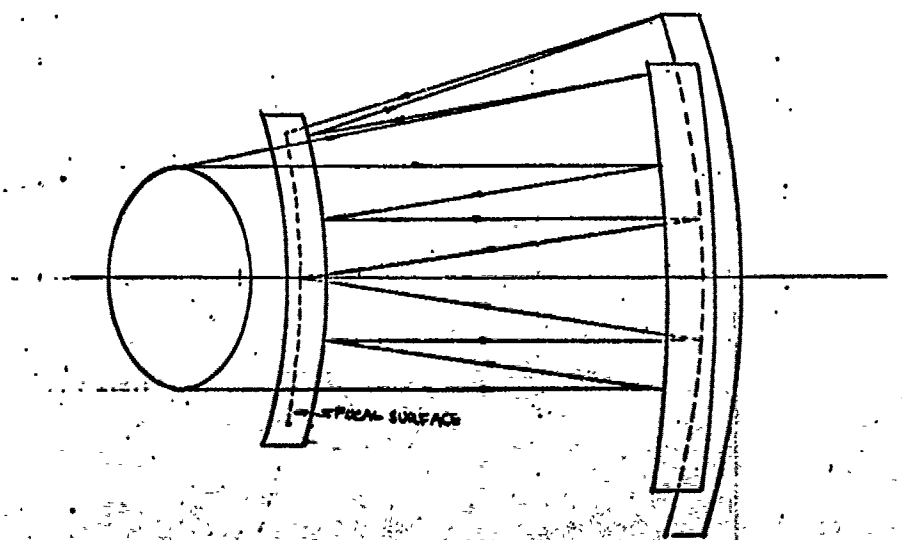

3- ASPHERIC UNOBSCURED APERTURE
0% VIGNETTING

FIGURE 10

LARGE-FIELD INFRARED SYSTEM		
SCALE 1"= 4CM	APPROVED BY:	DRAWN BY:
DATE: 7 MAR 71		APPROVED
ALL-REFLECTIVE / UNOBSCURED		
22° FIELD		DRAWING NUMBER

Figure 9 can be used in either the mirror scan mode or the detector scan. In the first case the scanning flat is placed in front of the system aperture as shown dotted in Fig. 9. In this mode, mirror No. 3 becomes a strip mirror rather than circularly symmetric as shown. In the case of detector scan, the detector array is located outside the beam where the scanner design is relatively uninhibited by interference with the optical beam.

In terms of optical performance and size we believe that the three-aspheric inverted Cassegrain with scanning flat is the most likely to meet the optical requirements, but we still ha a large scanning flat and associated problems.

Three-Aspheric Unobscured Cassegrain

In desperation we should look at something that seems quite a departure from convention. Let us see where we have been thwarted in the search for a satisfactory design. First we encountered a materials problem, and to solve it we would need to mount a major development problem for large water-free quartz or silica. The all-reflective systems pose us with learning how to fabricate asymmetric aspherics, and even then the required development program would leave us with a poor optical design. The other design requires a large scanning flat, and we would need a major developmental program to stretch lightweight mirrors at least an order of magnitude over today's state of the art. Since we could do this and still not have a good solution, why not depart drastically in only one area and see if a developmental program might be the answer here? We refer to the fabrication of off-axis sections of aspherics.

Figure 10 shows a surprisingly small and simple three-mirror design that has zero vignetting. The scanning mirror is now the stop, hence the smallest possible size for the 1-m aperture. Each of the other mirrors is a strip mirror but an off-axis section of an aspheric. The design that we have shown is very compact, and the optical aberrations even with three aspherics may not handle this case, but we can easily stretch the length of the group and improve the aberrations. The basic question is: do we want to consider such optical surfaces?

The mirror sections of this system will require new methods of fabrication, testing, and alignment techniques. Since it looks as if the proposed design stretches the art in other ways, this avenue may be the easiest. Several optical manufacturers have already probed this question, and we feel that more effort will get results that will be useful to both this and other programs requiring new optical capabilities.

Appendix II. RISLEY PRISM SCAN PATTERNS

Searching a field of view with a single infrared detector or detector array requires the use of some mechanical or optical device to provide the scan motion.

The Risley prism scanner is an example of a versatile optical method that can be used for small fields at high scanning rates.

Let us quickly review the refraction of a light ray passing through a prism. From Fig. 1 it can be seen that

$$D = I_1 + I_2 - A$$
$$A = I_1' + I_2'. \tag{1}$$

It is a simple matter to show that setting

$$dD/dI_1 = 0 \tag{2}$$

yields

$$I_1 = I_2 \quad \text{and} \quad I_1' = I_2' \tag{3}$$

as the condition for the deviation to be a minimum.

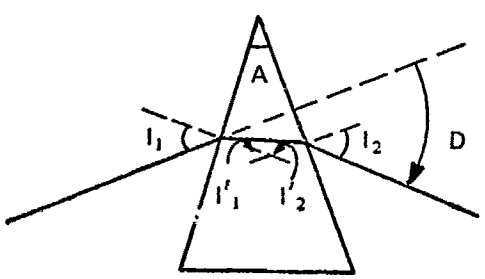

Fig. 1. Refraction by prism.

Now applying Snell's law to the prism surface, we obtain

$$N = \sin\tfrac{1}{2}(A + D_{min})/\sin\tfrac{1}{2}A. \tag{4}$$

This familiar expression is often used to determine the index of refraction of a material by measuring the angle of minimum deviation.

For a *thin prism* we can use the small angle approximation and

$$N \cong (A + D_{min})/A. \tag{5}$$

Also for thin prisms, the condition for the deviation to be a minimum, $I_1 = I_2$ and $I_1' = I_2'$, is always satisfied regardless of the orientation of the prism (i.e., the deviation is the same for a wide range of angles of incidence). Hence we drop the subscript and rearrange the above equation to obtain an expression for the deviation of a ray caused by a thin prism

$$D = (N - 1)A. \tag{6}$$

The *direction* of the deviation obviously depends upon the orientation of the prism; hence *phasor* (complex-valued functions of real variables) notation is convenient (Fig. 2). The magnitude and direction of the deviation is now expressed by

$$D = (N - 1)Ae^{j\phi}. \tag{7}$$

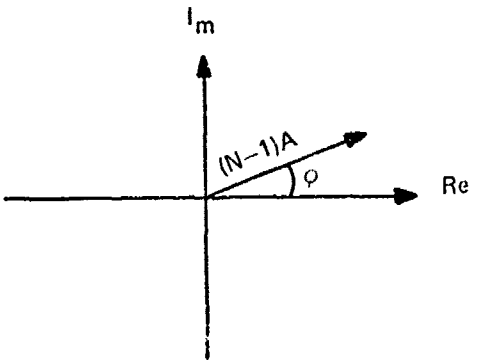

Fig. 2. Phasor diagram.

If we have a sequence of thin prisms the deviations add vectorially. Hence two thin prisms are equivalent to a prism whose power can be varied between the sum and the difference of the powers of the individual prisms (Fig. 3). Such variable power prisms have long been used by ophthalmologists for testing vision.

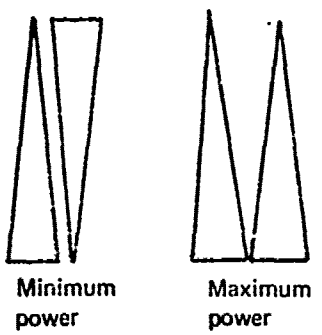

Fig. 3. Prism arrangement for minimum to maximum power.

If we now consider the case of two rotating thin prisms, we have

$$\begin{aligned} D_1 &= (N_1 - 1)A_1 e^{i(\omega_1 t+\phi_1)} \\ D_2 &= (N_2 - 1)A_2 e^{i(\omega_2 t+\phi_2)} \end{aligned} \tag{8}$$

and

$$D = D_1 + D_2 = (N_1 - 1)A_1 e^{i(\omega_1 t+\phi_1)} + (N_2 - 1)A_2 e^{i(\omega_2 t+\phi_2)}. \tag{9}$$

The deviation of a ray passing through two thin prisms rotating with angular velocities ω_1 and ω_2 is thus described by Eq. (9) and is seen to be a function of time and the initial orientation of the prisms.

Thus for two *identical* thin prisms, $N_1 = N_2 = N$, $A_1 = A_2 = A$, $\phi_1 = 0$, and $\phi_2 = \phi$, and we obtain for the deviation the expression

$$D = (N - 1)A[e^{i\omega_1 t} + e^{i(\omega_2 t+\phi)}] \tag{10}$$

where ϕ is the relative angle between the prisms at $t = 0$.

Let us now look at some special cases:

(a) $\omega_2 = \omega_1, \quad \phi = 0;$

therefore

$$D = 2(N - 1)Ae^{i\omega_1 t} \tag{11}$$

and a *circular scan* is produced. When $\phi \neq 0$, the radius of the circle (and starting point) changes

(b) $\omega_2 = -\omega_1, \quad \phi = 0;$

therefore

$$D = 2(N - 1)A \cos(\omega_1 t)$$

and a *line scan* is produced. When $\phi \neq 0$, the orientation of the line changes. This pattern is often used in conjunction with a linear array of detectors to cover a two-dimensional field

(c) $\omega_2 = -2\omega_1, \quad \phi = 0;$

therefore

$$D = 2(N - 1)Ae^{i(\omega_1 t/2)} \cos(3\omega_1 t/2)$$

and a *three-leaved rosette pattern* is produced

(d) $\omega_2 = \omega_1 \pm \Delta\omega, \quad \phi = 0, \quad \Delta\omega \ll \omega_1;$

therefore

$$D = (N - 1)Ae^{i\omega_1 t}(1 + e^{\pm i\Delta\omega t})$$

and a *spiral pattern* is produced. This is probably the simplest pattern to cover the entire two-dimensional field of view with a single detector. It can thus be utilized to considerable advantage in some infrared scanning systems (F. A. Rosell, "Prism scanner," J. Opt. Soc. Am. 50:521, 1960).

Of course there are many more possible scan patterns. In fact, Eq. (10) describes a complete three-parameter family of curves, similar in many respects to the well-known set of Lissajous figures. A few of these patterns are shown in Figs. 4 and 5.

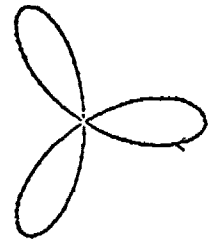

$\omega_2 = -2\omega_1, \phi = 0$

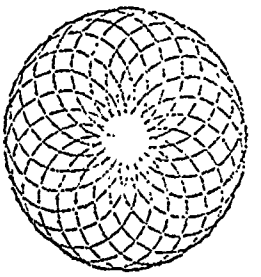

$\omega_2 = -20\omega_1, \phi = 0$

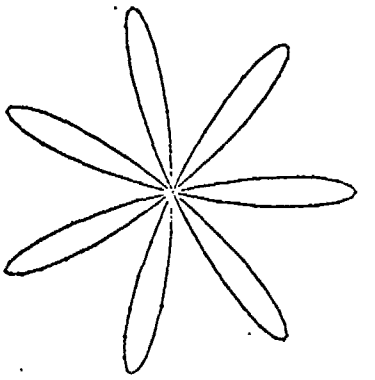

$\omega_2 = -4/3\,\omega_1, \phi = 0$

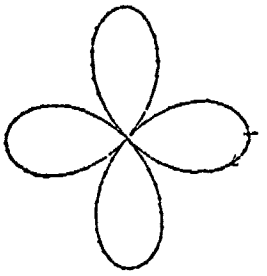

$\omega_2 = -3\omega_1, \phi = 0$

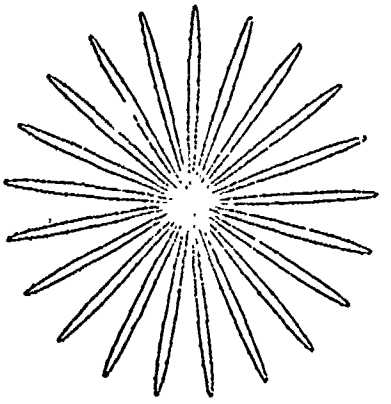

$\omega_2 = -1.1\omega_1, \phi = 0$

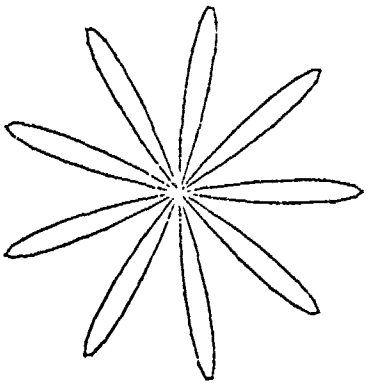

$\omega_2 = -5/4\,\omega_1, \phi = 0$

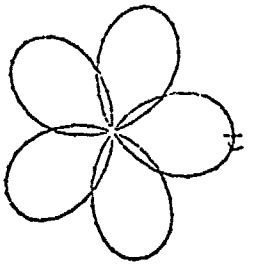

$\omega_2 = -4\omega_1, \phi = 0$

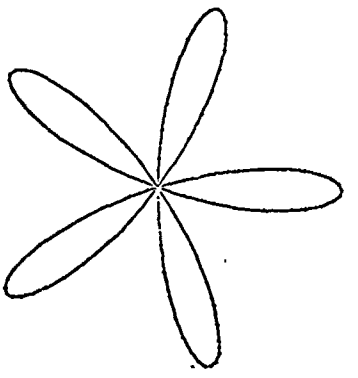

$\omega_2 = -3/2\,\omega_1, \phi = 0$

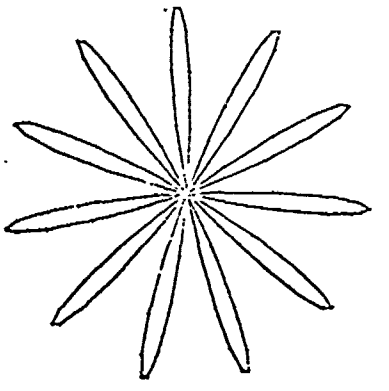

$\omega_2 = -6/5\,\omega_1, \phi = 0$

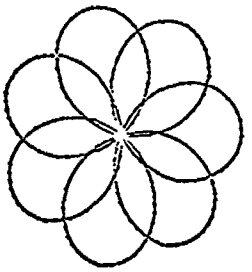

$\omega_2 = -6\omega_1, \phi = 0$

Fig. 4. Rosette patterns for Risley prism scan.

$\omega_2 = 2\omega_1, \phi = 0$

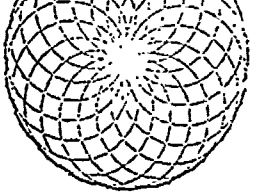

$\omega_2 = 20\omega_1, \phi = 0$

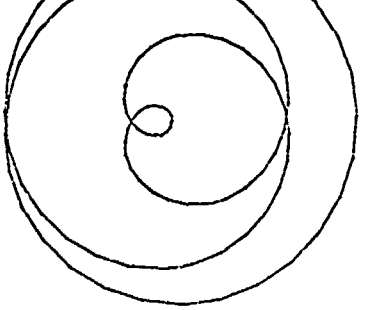

$\omega_2 = {}^4/_3\omega_1, \phi = 0$

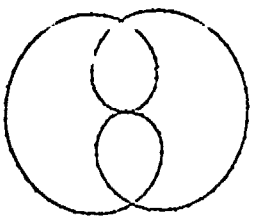

$\omega_2 = 3\omega_1, \phi = 0$

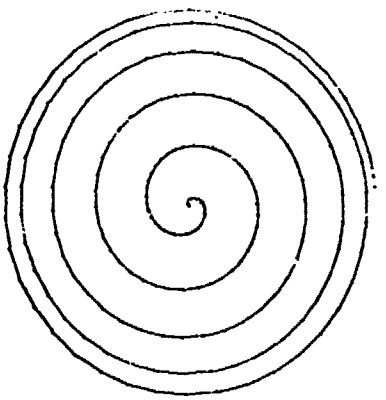

$\omega_2 = 1.1\omega_1, \phi = 0$

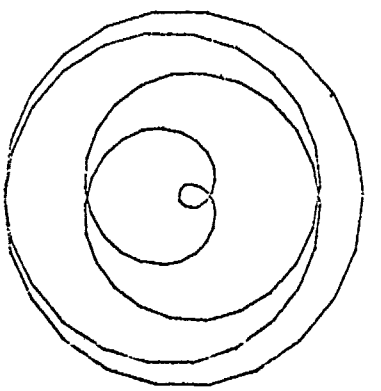

$\omega_2 = {}^5/_4\omega_1, \phi = 0$

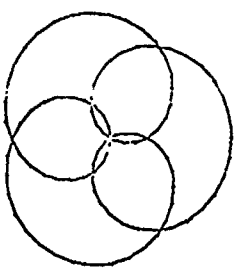

$\omega_2 = 4\omega_1, \phi = 0$

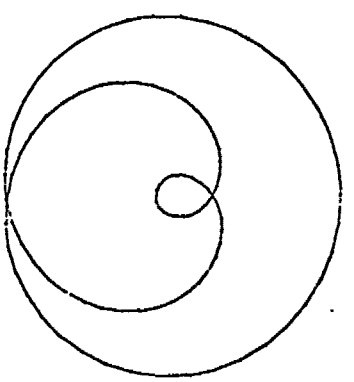

$\omega_2 = {}^3/_2\omega_1, \phi = 0$

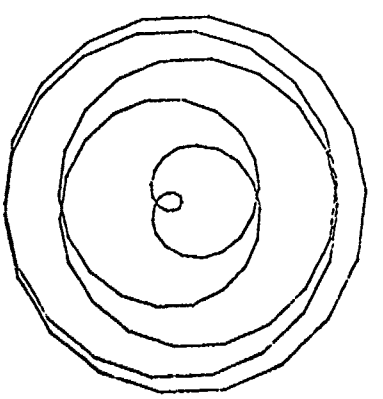

$\omega_2 = {}^6/_5\ \omega_1, \phi = 0$

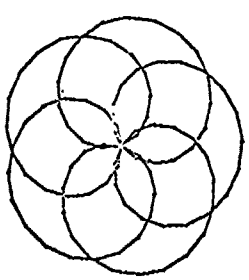

$\omega_2 = 6\omega_1, \phi = 0$

Fig. 5. Spiral patterns for Risley prism scan.

ACKNOWLEDGMENTS

Many of the considerations in this report are based upon the discussion of large-angle optical systems that is included as Appendix I. We are indebted to Dr. Aden B. Meinel for this work.

We would like to thank Theodore R. Whitney of Pacific Infrared Systems Company who was responsible for the Oscillating/Rotating Mirror.

UNCLASSIFIED
Security Classification

DOCUMENT CONTROL DATA - R & D

(Security classification of title, body of abstract and indexing annotation must be entered when the overall report is classified)

1 ORIGINATING ACTIVITY (Corporate author) Optical Sciences Center The University of Arizona Tucson, Arizona 85721	2a. REPORT SECURITY CLASSIFICATION UNCLASSIFIED 2b. GROUP

3 REPORT TITLE

(4) Large-Aperture Wide-Angle Infrared Scanning System.

4 DESCRIPTIVE NOTES (Type of report and inclusive dates)

(9) Final Contract Report, 1 Jun[redacted]71 through 31 Jan[redacted]72

5. AUTHOR(S) (First name, middle initial, last name)

(10) William L. Wolfe, James E. Harvey, Ben C. Platt

6 REPORT DATE	7a. TOTAL NO. OF PAGES	7b. NO. OF REFS
(11) Mar[redacted]72 (12) 64 p.	44	

8a. CONTRACT OR GRANT NO.	9a. ORIGINATOR'S REPORT NUMBER(S)
(15) F04701-71-C-0311 new	(14) OSC[redacted]-5010-4951-38-1
b. PROJECT NO.	
c.	9b. OTHER REPORT NO(S) (Any other numbers that may be assigned this report)
d.	(18) SAMSO TR-72-78 (19)

10 DISTRIBUTION STATEMENT

Distribution limited to U. S. Government Agencies only, test and evaluation, 15 January 1972. Other requests for this document must be referred to HQ SAMSO/SYAX, AFUPO, Los Angeles, California 90045.

11. SUPPLEMENTARY NOTES	12 SPONSORING MILITARY ACTIVITY
	Dept. of the Air Force Hq. Space & Missile Systems Orgn. (AFSC) Air Force Unit Post Office Los Angeles, California 90045

13. ABSTRACT

This final report covers a study performed at the University of Arizona concerning large-aperture, wide-angle infrared scanning systems. Both image-plane and object-plane scanning systems were investigated. Two configurations were developed in considerable detail and were shown to present feasible solutions to the specified problem. Laboratory models of these two scanning systems have been constructed to demonstrate the principles involved.

(402 821)

DD FORM 1 NOV 65 1473 (PAGE 1)
0102-014-6600

UNCLASSIFIED
Security Classification

14 KEY WORDS	LINK A		LINK B		LINK C	
	ROLE	WT	ROLE	WT	ROLE	WT
Large-aperture wide-angle infrared scanning system Optical Sciences						